Eindhoven University of Technology

MASTER

Towards the computation of the dynamic behaviour of rubber materials

de Bever, J.J.M.

Award date:
1992

Link to publication

Disclaimer
This document contains a student thesis (bachelor's or master's), as authored by a student at Eindhoven University of Technology. Student theses are made available in the TU/e repository upon obtaining the required degree. The grade received is not published on the document as presented in the repository. The required complexity or quality of research of student theses may vary by program, and the required minimum study period may vary in duration.

General rights
Copyright and moral rights for the publications made accessible in the public portal are retained by the authors and/or other copyright owners and it is a condition of accessing publications that users recognise and abide by the legal requirements associated with these rights.

- Users may download and print one copy of any publication from the public portal for the purpose of private study or research.
- You may not further distribute the material or use it for any profit-making activity or commercial gain

Towards the computation of the dynamic behaviour of rubber materials

WFW-report 92.007

Anniek de Bever

10-01-1992

Abstract

In this work, two constitutive equations, describing the three-dimensional behaviour of a nonlinear viscoelastic rubber material are investigated: the multi mode upper-convected Maxwell model and Lianis' constitutive equation for small strains superposed on a finite deformation. The first model has been implemented in the finite element package SEPRAN by adapting an existing one mode Maxwellian element. The latter model is available in the finite element package MARC.

The material parameters occuring in these theories have been obtained for both a butyl rubber, code K1043, and a silicone rubber, code sil40H, with use of linear dynamic shear experiments and non linear stress relaxation experiments.

Comparison of numerical simulations with experimental data, shows that the multi-mode Maxwell model is able to describe the degree of non-linearity in tension in the strain domain [0,70]%. Furthermore, it predicts qualitatively the Mullins effect. In order to better evaluate the predictive qualities of the multi mode Maxwell model, more experimental data of hysteresis curves in uniaxial tension and compression should be obtained.

Numerical simulations with the finite element code MARC showed that Lianis' constitutive equation was not correctly implemented in this package. Future attention should be focussed on the predictive quality of transfer functions, for different geometries, obtained with MARC. If the results are satisfactory a powerfull tool for the design of rubber dampers is obtained.

Preface

This project was performed in the Continuum mechanics, Systems & Control and Tribology group at the Philips Research Laboratories in Eindhoven, The Netherlands. This is the thesis work for the degree of master of science from the University of Technology in Eindhoven.

I would like to to acknowledge the support and guidance of my coach Frank Baaijens during this work. I would like to thank Leon Govaert for the many helpfull discussions and his support with the experiments. Also I would like to thank Wim Zoetelief and Gerrit Peters for their help with the measurements of the linear viscoelastic properties of the materials. Furthermore I would like to acknowledge the PMF for providing the rubber materials on which I have conducted the experiments. My sincere thanks are also due to all members of the group 'Sastra', especially Peter van Hoogstraten and Willem Potze, who have contributed with their work and suggestions to this project, and who provided a very nice working environment.

Anniek de Bever

Contents

1 Introduction 4
- 1.1 Overview . . . 4
- 1.2 Literature survey . . . 5
- 1.3 Layout of the report . . . 7

2 Constitutive equations 8
- 2.1 Introduction . . . 8
- 2.2 The multi-mode Maxwell model . . . 8
- 2.3 Lianis's theory . . . 9

3 Stress relaxation measurements 12
- 3.1 Principle for stress relaxation measurement . . . 12
- 3.2 Experimental . . . 13
- 3.3 Results and discussion . . . 13

4 Dynamical measurements 18
- 4.1 Introduction . . . 18
- 4.2 Experimental . . . 19
- 4.3 Time-temperature superposition . . . 19
- 4.4 Modelling . . . 22
- 4.5 Model verification . . . 26
- 4.6 Non-linearity in shear . . . 31

5 Results of numerical simulations 35
- 5.1 Introduction . . . 35
- 5.2 Hysteresis curves of butyl and silicone rubber . . . 35
- 5.3 Transfer functions of butyl and silicone rubber . . . 36

6 Conclusions and Suggestions 38

A Basic principles of continuum mechanics 44
- A.1 Introduction . . . 44
- A.2 Kinematics of a continuum . . . 44

A.3 Balance laws 46
A.4 Constitutive principles 47

B The Mullins effect 49

C Sinusoidal small-amplitude vibrations superposed on finite deformation in viscoelastic solids 51

D Relaxation functions 55

E The material behaviour of elastomers in MARC 57

F The Maxwell model in stress relaxation 59

G The rheometrics RDS-2 61

H The WLF equation 63

I Derivation of the discrete viscoelastic spectra 66

J Results of preleminary DMTA and DSC eperiments 68

K Hysteresis curves in uniaxial tension 72

L Hysteresis curves in uniaxial compression. 75

M Derivation of the transfer function for a Maxwell element 79

N Bode plots of butyl and silicone rubber 82

Chapter 1

Introduction

1.1 Overview

The use of rubber materials in engineering applications has increased markedly in the last three decades. One of these applications is the use of passive rubber dampers for the suspension of the laser module inside an outdoor CD-player. So far there are no design rules to create rubber dampers with required damping properties. As a consequence the design process has been empirical. This means that costly design iterations have to be performed, which involve design, testing and redesign.

To facilitate the design process, it is desirable to have an analysis tool to simulate the mechanical behaviour of rubber components. Essentially this requires some form of theory to model the material behaviour, experimental methods to measure the material parameters occuring in the theory, and numerical methods to perform the calculations.

Initial investigations have shown that rubber dampers cannot be modelled by simple linear viscoelastic theories. Therefore two non-linear viscoelastic theories, derived from literature, are applied. Calculations are performed with use of the finite element method. The first material model used is a so-called multimode Maxwell model. It has been implemented in the finite element package SEPRAN by adapting a one mode upperconvected Maxwell model. The second theory applied is based on the theory of Lianis, who derived a constitutive equation which describes the behaviour of incompressible solids if a small deformation is superposed on a static finite deformation field. A specialized form of this theory is available in the finite element package MARC. The material parameters, used in these theories, are measured by linear viscoelastic shear measurements, and stress relaxation measurements.

1.2 Literature survey

This section summarizes the present state in research concerning the dynamic behaviour of rubber materials. It is mainly focused on available constitutive equations for the mechanical behaviour of rubbers. A complete overview is given in [6].

Linear theory of viscoelasticity

In the early development of viscoelasticity theory, much use was made of the modelling of materials by networks made up of springs and dashpots. The spring represents the elastic component of the material, whereas the dashpot represents the viscous component. An overview of some simple combinations of springs and dashpots and their constitutive equations can be found in i.e. reference [6]. More general mechanical models are obtained by combination of an arbitrary number of elements. These models are refered to as canonical models [1]

The mechancial models mentioned above represented the one-dimensional response behaviour of a linear viscoelastic material. A linear infinitesimal theory of viscoelasticity for three-dimensional behaviour is given by i.e. Lockett [29].

Nonlinear elasticity

The theory of nonlinear elasticity is of interest because at the limits of the time and frequency range, viscoelastic solids essentially behave elastic.

Based upon the molecular structure of rubber, general expressions for the deformation of rubber units can be derived. Contributions in this field worth mentioning are the statistical or kinetic theory, which is in extension valid untill about 30 % strain, [45] and the non-Gaussian theory, which takes the finite extensibility of the network chains into account [12], pages 155-178.

In parallel with the statistical theory of rubber elasticity, the phenomenological theory was derived. This theory aims at providing a mathematical framework for all materials which are capable of large elastic deformations, and is not concerned with the molecular structure. Work in this field was initiated by Mooney and continued by Rivlin [15]. Their constitutive equation is known as the Mooney-Rivlin equation, and is valid up to 250 % in extension, but does not describe uniaxial compression data well with the same constants. More in accordance with experimental data are the Ogden [33], Valanis-Landel [46] and the Peng [35] material models.

Integral constitutive equations for nonlinear viscoelastic material behaviour

Green and Rivlin [38] expressed the three-dimensional behaviour of a viscoelastic isotropic solid as the sum of a series of multiple integrals. Even in the third-order

approximation of this theory, a large number of experimental tests is required in order to determine the material functions. Furthermore the third order approximation is restricted to small strain or stress rates and to nonlinear materials which do not differ much from their linear counterparts. In addition Pipkin and Rogers [37] developed a multiple integral constitutive equation that is non-linear even in its first term approximation. Their motivation was that the first integral term should model single step tests exactly, the second term should extend the exact representation to two step tests etc. Experimental determination of the material functions requires a large number of tests, unless the material is completely characterizable in a one step test.

Schapery [40] developed stress-strain equations for nonlinear, initially isotropic, viscoelastic materials with constant temperature by extending Biot's linear thermodynamic theory. However it is difficult to apply these equations to specific problems and to simple configurations which are used in material property evaluation.

Integral theories that do not require a large experimental program include the theories of Bernstein, Kearsley and Zapas [29], Bloch, Chang and Tshoegl [9, 10] and, the finite linear viscoelasticity theory of Coleman and Noll [29]. Lianis [27] derived the theory of small viscoelastic motion superposed on large static deformation using the general equation of Coleman and Noll. This theory is implemented by Morman and Nagtegaal [31] in the commercially available finite element package MARC

Differential and rate type models for nonlinear viscoelastic material behaviour

Constitutive equations of the rate or differential type found in literature are commonly used to describe the behaviour of nonlinear viscoelastic fluids rather than that of nonlinear viscoelastic solids.

A much used rate type model is the upperconvected Maxwell equation. Its integral equivalent is called the Lodge equation and results from the molecular model of Green and Tobolsky [23]. A more realistic model is obtained by considering a generalized or multi-mode Maxwell model, which contains n relaxation times and n viscosities ($n > 1$). A modification of the upperconvected Maxwell model has been introduced by White and Metzner [48]. In their model the relaxation times and viscosities depend on the rate of strain.

The Giesekus model is based on a kinetic theory of closely packed polymer chains and on a series of simplifications. It contains an adjustable parameter α. When $\alpha = 0$ the upperconvected Maxwell model is recovered [23]. Leonov's constitutive equation [24, 25, 26] in its simplest form is similar to the Giesekus model,but is derived from a thermodynamic rather than a molecular approach. The basic assumption underlying his theory is given by the principle of relaxability in the small [2].

A model which obeys time strain separability has been proposed by Larson [23].

Like the Giesekus model it contains an adjustable parameter α, and also for $\alpha = 0$ the upperconvected Maxwell model is retrieved. However as with the Giesekus equation the value of α that would best fit the uniaxial data is less than that which would give the best fit to the shear data [21]

Phan-Thien and Tanner [36] derived a constitutive equation from a Lodge-Yamamoto type of network for polymeric fluids. They allowed the network to have a certain slip and assumed that the rate of creation and destruction of the network depends on the instantenous elastic energy of the network.

1.3 Layout of the report

In this section the layout of this report is presented.

Chapter 1 - General introduction and literature survey.

Chapter 2 - Presentation of the used equations, describing the material behaviour of rubber.

Chapter 3 - Stress relaxation measurements in uniaxial tension.

Chapter 4 - Dynamical measurements in shear.

Chapter 5 - Results of numerical simulations.

Chapter 6 - The main results obtained from this work are summarized and suggestions are given for further research.

Chapter 2

Constitutive equations

2.1 Introduction

In this chapter, two constitutive equations, which describe the behaviour of a rubber material are presented. The rubber is considered as a continuum. The basic concepts of continuum mechanics are summarized in appendix A. For more details the reader is referred to i.e. Eringen [13]

In section 2.2 the multimode Maxwell model is presented. This model is chosen from literature because it describes the degree of nonlinearity adequately for the stress-strain domain investigated. Furthermore this model is capable of describing the Mullins effect. The latter is explained in appendix B.

In section 2.3 Lianis's theory is presented. It describes the behaviour of a rubber unit loaded with a small amplitude time harmonic oscillation superposed on a static finite deformation. This model is available in the finite element package MARC. It has the advantage that it provides the deflections and stresses as a function of the frequency.

2.2 The multi-mode Maxwell model

The upperconvected Maxwell model describes the material behaviour of a viscoelastic isotropic incompressible material. It is given by:

$$\left.\begin{array}{rcl} \boldsymbol{\sigma} & = & -p\mathbf{I} + \boldsymbol{\tau} \\ \overset{\nabla}{\boldsymbol{\tau}} + \frac{1}{\theta}\boldsymbol{\tau} & = & \frac{2\eta}{\theta}\mathbf{D} \end{array}\right\} \tag{2.1}$$

where: $\boldsymbol{\sigma}$ is the Cauchy stress tensor.
p is an isotropic constant.
$\mathbf{I}$ is the unity tensor.
$\boldsymbol{\tau}$ is the extra stress tensor.
$\overset{\nabla}{\boldsymbol{\tau}}$ is the Truesdell rate of the extra stress tensor.

θ is a time constant.
η is a viscosity.
$\mathbf{D}$ is the rate of deformation tensor.

The Truesdell rate of the extra stress tensor, occuring in the upperconvected Maxwell model is defined by:

$$\overset{\nabla}{\boldsymbol{\tau}} = \dot{\boldsymbol{\tau}} - \mathbf{L}\cdot\boldsymbol{\tau} - \boldsymbol{\tau}\cdot\mathbf{L}^c \tag{2.2}$$

where $\mathbf{L}$ is the velocity gradient tensor.

The predictive quality of the upperconvected Maxwell model is enlarged by considering a multi-mode model containing n viscosities η_i and n relaxation times θ_i. This so-called generalized upperconvected Maxwell model is given by:

$$\left.\begin{array}{rcl} \boldsymbol{\sigma} & = & -p\mathbf{I} + \sum_i^n \boldsymbol{\tau}_i \\ \overset{\nabla}{\boldsymbol{\tau}}_i + \frac{1}{\theta_i}\boldsymbol{\tau}_i & = & \frac{2\eta_i}{\theta_i}\mathbf{D} \end{array}\right\} \tag{2.3}$$

The deformation of a body is described mathematically by combining the balance laws (see appendix A, section A.3) and the constitutive equations. The multi-mode Maxwell model is implemented in teh finite element package SEPRAN by modifying the results of [5].

The parameters η_i and θ_i can be determined by measuring the linear viscoelastic material functions only.

2.3 Lianis's theory

In this section a method is presented for the isothermal mechanical analysis of incompressible viscoelastic materials, in which a small-amplitude time harmonic oscillation with frequency ω is superposed on a static finite deformation field. The material behaviour is assumed to be of the 'fading memory' type, so that when it is held at a constant deformation, the stresses eventually relax to equilibrium values that depend only on the current state of deformation. The constitutive equation taken as a starting point is that of Lianis [27], who derived the theory of small motion superposed on large static deformations using the finite linear viscoelasticity theory of Coleman and Noll. In appendix C the Fourier transform of the Lianis constitutive equation in terms of the second Piola Kirchhoff stress and the Lagrangian strain has been derived, and is given by:

$$\mathbf{S} = \mathbf{S}^0 + \Delta\mathbf{S}^* \exp(i\omega t) \tag{2.4}$$

Where the superscript * denotes a complex-valued function of frequency ω. In the above equation $\mathbf{S}^0$ is the static equilibrium second Piola Kirchhoff stress tensor, defined by:

$$\mathbf{S}^0 = -p^0\,(\mathbf{C}^0)^{-1} + 2[W_1\mathbf{I} + W_2(I_1^0\mathbf{I} - \mathbf{C}^0)] \tag{2.5}$$

where: p_0 is an arbitrary scalar, arising as a reaction to the constraint of material incompressibility.

$\mathbf{C}^0$ is the right Cauchy-Green tensor of the static finite deformation.

I_1^0, I_2^0 are, respectively, the first and second invariants of $\mathbf{C}^0$.

$W(I_1^0, I_2^0)$ is the equilibrium value of the Helmholtz free energy density measured per unit volume of the undeformed body.

W_i is defined as $\frac{\partial W}{\partial I_i}$, $(i = 1, 2)$.

Furthermore the stress-increment $\Delta\mathbf{S}^*$ due to the superposed harmonic displacement is given by:

$$\Delta\mathbf{S}^* = -\Delta p^*(\mathbf{C}^0)^{-1} + {}^4\mathbf{L}^* : \Delta\boldsymbol{\epsilon}^* \tag{2.6}$$

where the quantity Δp is an arbitrary scalar arising as a reaction to the superposed material motion, $\Delta\boldsymbol{\epsilon}$ denotes the superposed strain increment and ${}^4\mathbf{L}^*$ is a complex fourth-order tensor defined by:

$${}^4\mathbf{L}^* = {}^4\mathbf{D} + 2i\omega\,{}^4\boldsymbol{\Phi}^* \tag{2.7}$$

In the above equation ${}^4\mathbf{D}$ is the elasticity tensor and ${}^4\boldsymbol{\Phi}^*$ is the complex valued relaxation function due to the superposed time harmonic vibrations. Both tensors are defined in appendix C.

Morman [31] presents a simplification, based on the assumption that the material exhibits seperability of time and strain. This leads to explicit expressions for the nine complex valued scalar relaxation functions, which appear in the relaxation tensor. These functions can be determined with the use of the same material parameters η_i and θ_i as occuring in the previous section. In appendix D the relaxation functions are determined.

Morman and Nagtegaal [31] have implemented the above constitutive equation in the finite element package MARC. They formulated the equilibrium equations in terms of the virtual work equation. This equation is incomplete when the deformation is incompressible, because the incompressibility condition forms a constraint on the displacement field. This constraint is treated with use of Lagrange multipliers and the problem is formulated with the augmented virtual work equation. In order to avoid numerical instability due to dilatation, Morman and Nagtegaal formulated the incompressibility constraint as:

$$f(I_3) = 3(I_3^{\frac{1}{6}} - 1) = 0 \tag{2.8}$$

The Newton-Raphson iteration process is used to solve the equations. This means that starting from a given value of displacements, accelerations etc, denoted by the superscript n, new values, denoted by the superscript $n+1$ are searched. Thus:

$$\mathbf{E}^{n+1} = \mathbf{E}^n + \Delta\mathbf{E} \tag{2.9}$$

where $\Delta\mathbf{E}$ denotes the error in the estimate. This yields after linearization in the following finite element formulation:

$$\int_V \Delta\mathbf{S} : \delta\Delta\mathbf{E}\, dV + \int_V \mathbf{S}^n : \delta\Delta\boldsymbol{\eta}\, dV = R^{n+1} - \int_V \mathbf{S}^n \delta\Delta\boldsymbol{\epsilon}\, dV \tag{2.10}$$

$$\int_V \delta\Delta p[\frac{1}{3}(I_3^n)^{\frac{-5}{6}}(\mathbf{C}^n)^{-1}\Delta\boldsymbol{\epsilon} + (I_3^n)^{\frac{1}{6}} - 1]\, dV \tag{2.11}$$

In the above equation $\boldsymbol{\epsilon}$ denotes the linear part of the Green-Lagrange strain tensor and $\boldsymbol{\eta}$ denotes the nonlinear part of this tensor. It should be noted that V denotes the volume of the undeformed configuration. Furthermore the quantity R^{n+1} is defined as:

$$R^{n+1} = \int_{A_T} T^{n+1}\delta\Delta u\, dA + \int_V F^{n+1}\delta\Delta u\, dV - \int_v \rho_0 \ddot{u}^{n+1}\delta\Delta u\, dV \tag{2.12}$$

where ρ_0 is the material density per unit of undeformed volume, F is the distributed force per unit of of undeformed volume, T is the prescribed surface traction per unit undeformed area, A_T is that part of the undeformed surface of the body where surface tractions are applied and A is surface area of the body in the undeformed configuration.

After discretization the matrix formulation of equations (2.10) and (2.11) is obtained. It is this formulation which is available in MARC. A note on the use of this formulation is given in appendix E.

Chapter 3

Stress relaxation measurements

3.1 Principle for stress relaxation measurement

In a stress relaxation test the rubber is held at a constant strain and the load needed to maintain this strain is measured. Directly after applying the deformation, the retractive force usually declines rapidly because of conformational changes and alignment of polymer chains. After some time these effects no longer dominate the stress relaxation, especially not at higher temperatures, and it is mainly chemical degradation of the network that contributes to stress relaxation.

Stress relaxation measurements can be made in tension, compression or shear. The stress relaxation measurements described in this chapter, were conducted in uniaxial extension. In theory the strain is applied instantenously. Experimentally this is not possible, see figure 3.1. It takes a certain time t_0 to reach the desired strain level. Due to the more gradual increase of strain the respons is different from the instantenous one. However after approximately 10 times t_0 the respons is equal to the instantenous respons, see figure 3.2. Therefore it is not possible to determine the time constants for times smaller than t_0. These time constants have to be determined with the aid of dynamic measurements.

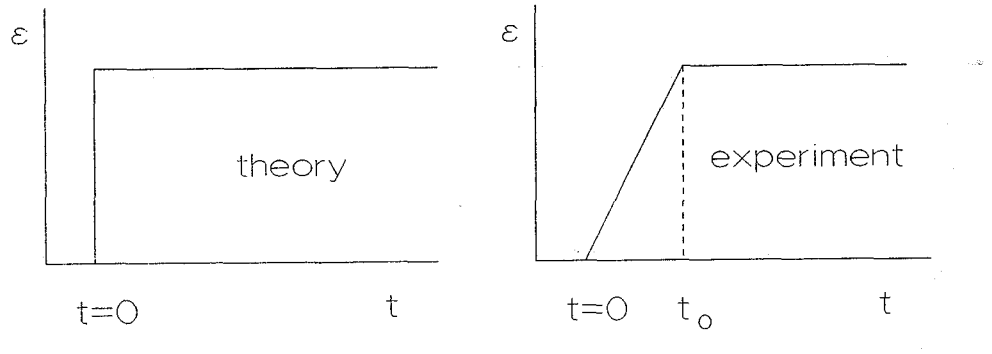

Figure 3.1: A step of strain in theory and in real life.

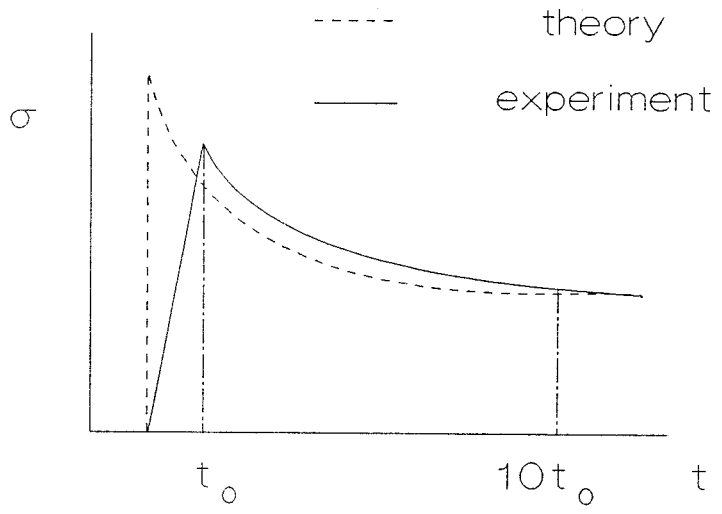

Figure 3.2: The respons on a step of strain in theory and in real life.

3.2 Experimental

Two types of rubber were used for the stress relaxation experiments, a butyl rubber code K1043 and a silicone rubber code sil40H. Both types were compounded at the PMF (Philips). The test specimens were dumb-bells cut from rubber sheets with thicknesses varying between 1.5 and 3.5 mm.

The experiments were conducted on a Frank 81565 tensile tester. Prior to testing all specimens were conditioned by subjecting them to a higher strain than they would experience during the testing. Because of the weakness of the rubber compounds a preload of 1 N was applied to the specimens. Then the extensiometer, which measured the strain, was installed. The desired strain could be attained in 10 seconds. The strain was held constant and the force needed to maintain this strain was constantly being recorded. The data was processed by computer, the program used to process the data was 'dataq'. All experiments were carried out at room temperature.

3.3 Results and discussion

Two sets of relaxation tests were conducted on the materials. In figures 3.3 and 3.4 the results of stress relaxation measurements in uniaxial tension are shown. Usually the testing gave a reproducibility of $\pm$ 10 %. This variation is due to several factors such as: the difficulty to define the zero point, the sample to sample variation, the ability to measure the sample dimensions accurarely, etc.

The average of the two sets of relaxation measurements is used to determine the isochronal stress/strain curve. At t = 500 seconds the average stress is crossplotted as a function of the strain. The results are shown in figure 3.5. These isochronal stress/strain curves do not cross the origin. This is caused by the fact that the

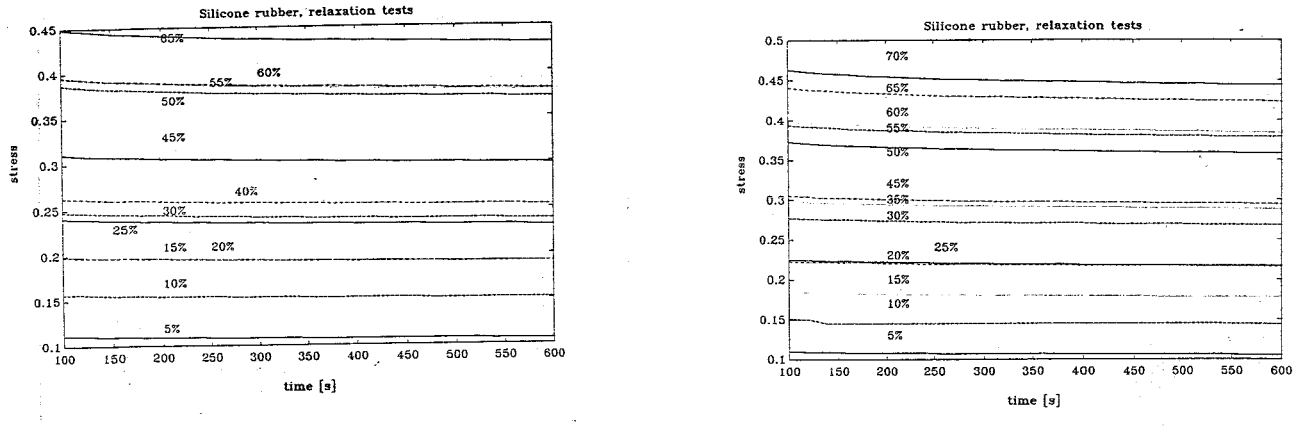

Figure 3.3: Response of silicone rubber to a step of strain at various stretch ratios as a function of time.

dumb-bells were preloaded (1 N) prior to testing. By extrapolating the curves to zero, followed by shifting them untill they cross the origin, the corrected curves are obtained.

The prediction of stresses from the upperconvected and generalized Maxwell models (see appendix F) has been fitted on the stress relaxation data of silicone and butyl rubber. The results are shown in figures 3.6 and 3.7. Obviously the generalized Maxwell model provides a better fit than the upperconvected Maxwell model. In figure 3.8 the prediction of the isochronal stress-strain curve from the generalized Maxwell model is compared with the isochronal stress-strain curves. It can be seen that the Maxwell model yields a good prediction of the reality for the considered strain domain.

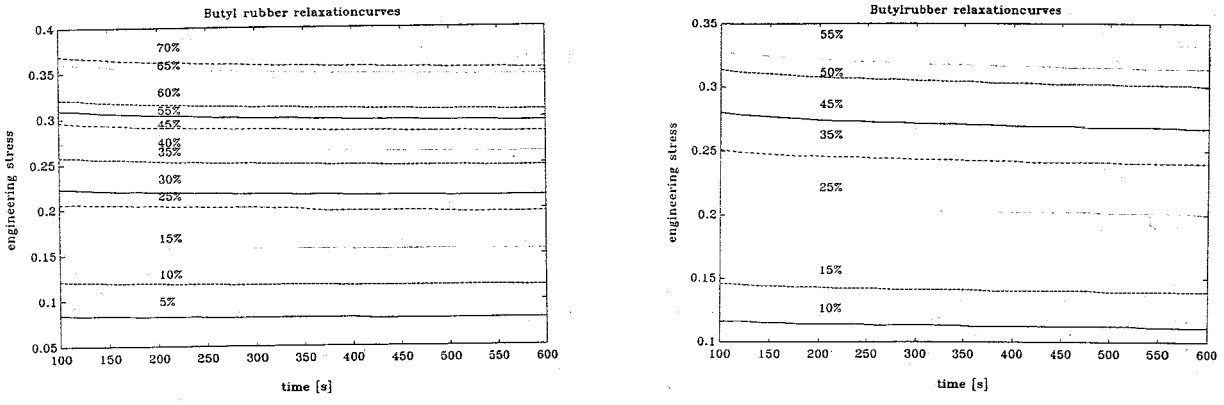

Figure 3.4: Response of butyl rubber to a step of strain at various stretch ratios as a function of time.

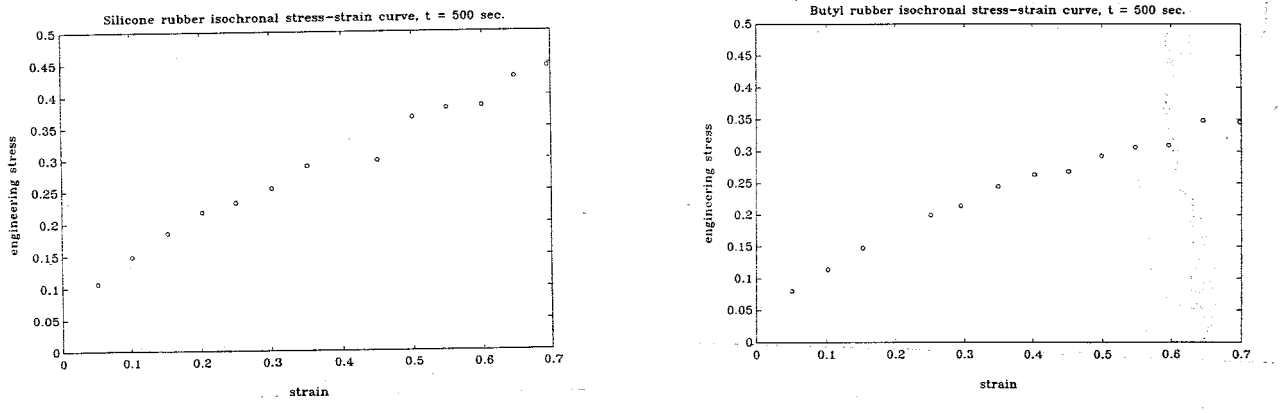

Figure 3.5: Isochronal stress-strain curves.

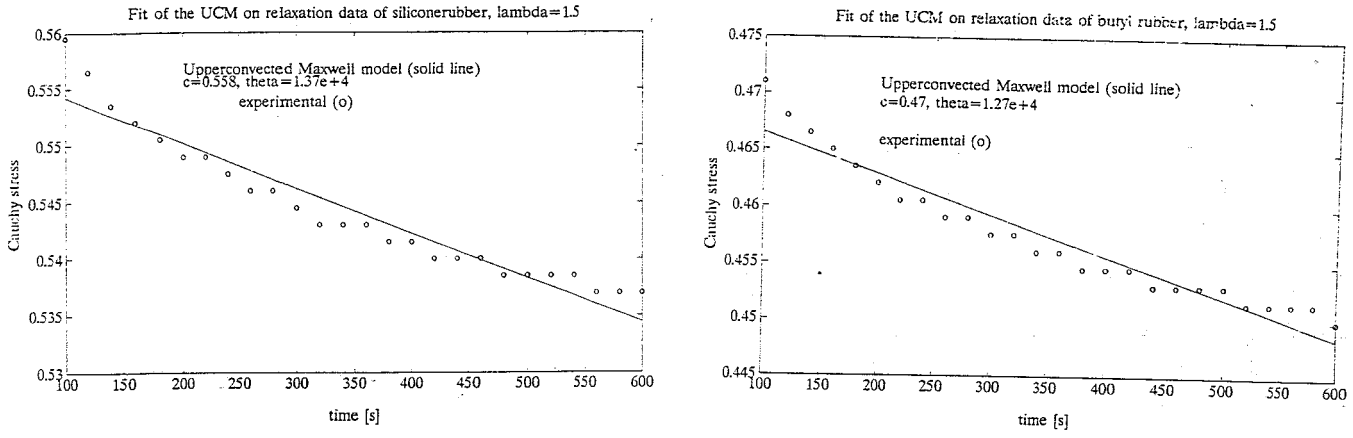

Figure 3.6: Fit of the upperconvected Maxwell model on relaxation data of silicone and butyl rubber.

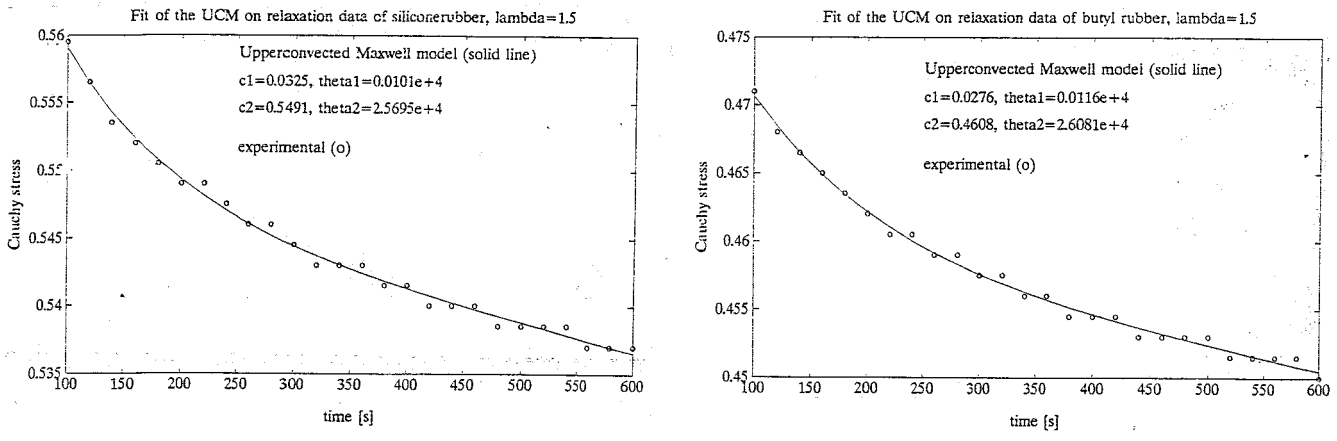

Figure 3.7: Fit of the generalized Maxwell model on relaxation data of silicone and butyl rubber.

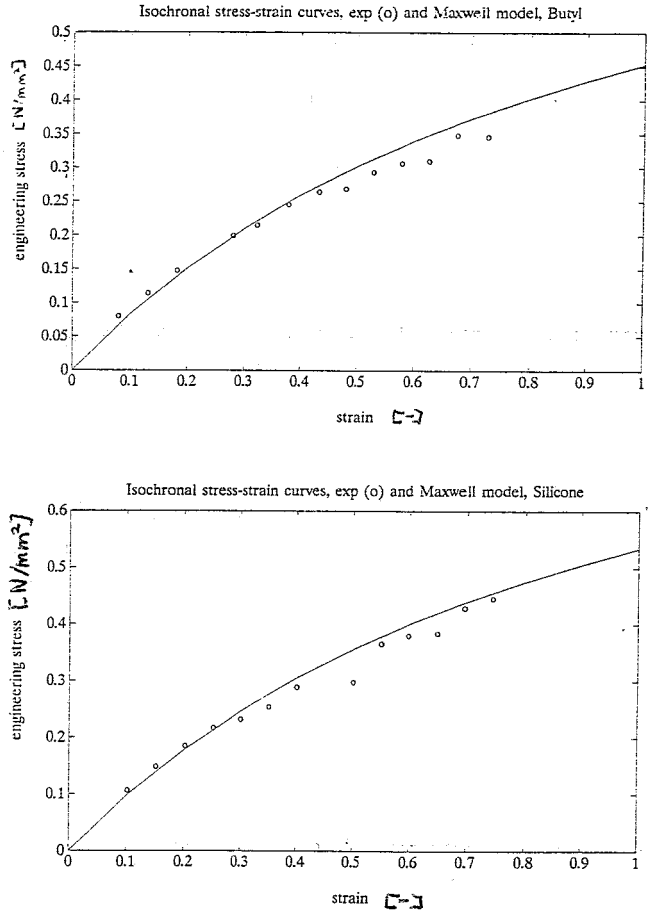

Figure 3.8: Comparisson of the isochronal stress-strain curve predicted from the generalized Maxwell model with the isochronal stress/strain curves of silicone and butyl rubber.

Chapter 4

Dynamical measurements

4.1 Introduction

The linear viscoelastic properties of the rubber compounds are measured by means of small amplitude torsional oscillatory shear experiments. The deformation is varied sinusoidally with an angular frequency ω. The input is of the form:

$$\gamma = \gamma_0 \cos(\omega t) = \gamma_0 \mathrm{Re}\{\exp(i\omega t)\} \tag{4.1}$$

where γ is the shear strain, γ_0 is the shear strain amplitude and t is the time. When the amplitude is small, the shear stress τ_{12} will be sinusoidal with frequency ω, but with a different amplitude and not in phase with the strain input.

$$\tau_{12} = \tau_0 \cos((\omega t) + \delta) = \tau_0 \mathrm{Re}\{\exp(i(\omega t + \delta))\} \tag{4.2}$$

The quotient of stress and strain gives the (frequency depended) complex shear modulus G^*:

$$G^*(i\omega) = \frac{\tau_0}{\gamma_0} \exp(i\delta) = G_d \exp(i\delta) \tag{4.3}$$

G^* can be split into a real component G', the so-called shear storage modulus, which is in phase with the strain (elastic respons) and an imaginary component G'',the loss modulus, which is $\frac{\pi}{2}$ radians out of phase with the strain input (viscous respons). Thus:

$$G^* = G' + iG'' \quad \Rightarrow \quad G' = \frac{\tau_0}{\gamma_0} \cos\delta \ \text{ and } \ G'' = \frac{\tau_0}{\gamma_0} \sin\delta \tag{4.4}$$

The ratio of the loss modulus to the storage modulus ($\tan\delta$) is a measure of the amount of elastic and/or viscous respons of the material. The loss angle δ is defined by:

$$\tan\delta = \frac{G''}{G'} \tag{4.5}$$

When δ approaches zero the viscoelastic material behaviour tends towards that of an elastic rubber whilst when δ approaches $\frac{\pi}{2}$ it tends towards that of a simple liquid [8] [11].

4.2 Experimental

The dynamic moduli are measured by means of small amplitude oscillatory shear experiments, conducted on a Rheometrics Dynamic Spectrometer RDS-2. In appendix G a short explanation is given concerning the RDS-2.

The polymers used are a silicone rubber (code sil40H) and a butyl rubber (code K1043). Both polymers were compounded at the PMF (Philips). The plate-and-cone geometry is employed. The silicone rubber has been vulcanized between the aluminium plate and cone. The primer used was Wacker Silicone G790. The butyl rubber could not be vulcanized on aluminium and therefore was glued with Loctite superbonder 495 between the discs. Because the glue also stuck on the side of the samples, a thin layer was taken off the samples by turning them on a lathe.

The experiments were conducted at temperatures between 223 K and 373 K. The micrometer reading of the sample thickness was corrected for the thermal expansion of the aluminium plate-and-cone and connecting shafts. The frequency varied between 0.1 and 500 rad/s. The experimental data are shown in figures 4.1, 4.2, 4.3 and 4.4. As expected the absolute value of the dynamic modulus $|G^*|$ increases for both silicone as well as butyl rubber with increasing frequency at a fixed temperature, and decreases with increasing temperature at a fixed frequency. On the other hand for silicone rubber the loss angle δ remains flat in the used temperature/frequency domain. For butyl rubber the loss angle δ initially increases with increasing temperature at a fixed frequency, reaches its maximum and subsequently decreases. This maximum is ascribed to the glass transition. At this so-called glass transition, elastomers exhibit rapidly increasing modulus through several orders of magnitude in a small temperature range. It is believed that the glass transition marks a loss in molecular mobility.

4.3 Time-temperature superposition

Thermorheological simple material behaviour is assumed, so time-temperature superposition can be applied. This means that the G^* and δ curves, measured at different temperatures can be shifted horizontally along the frequency axis into one master curve at a certain reference temperature T_0. The same value of the horizontal shift-factor a_{T_0} then superimposes all viscoelastic functions. Due to thermal expansion, a small additional vertical shift b_T is needed to superimpose the dynamic moduli. The master curves then can be described by [14]:

$$\delta(\log\omega, T) = \delta(\log\omega a_T(T, T_0), T_0) \tag{4.6}$$

$$|G^*(\log\omega, T)| = b_T(T, T_0)|G^*(\log\omega a_T(T, T_0), T_0)| \tag{4.7}$$

The best way to start a superposition procedure is to superimpose the $\delta(\log\omega)$ curves at various temperatures and to use the horizontal shift factors a_T obtained

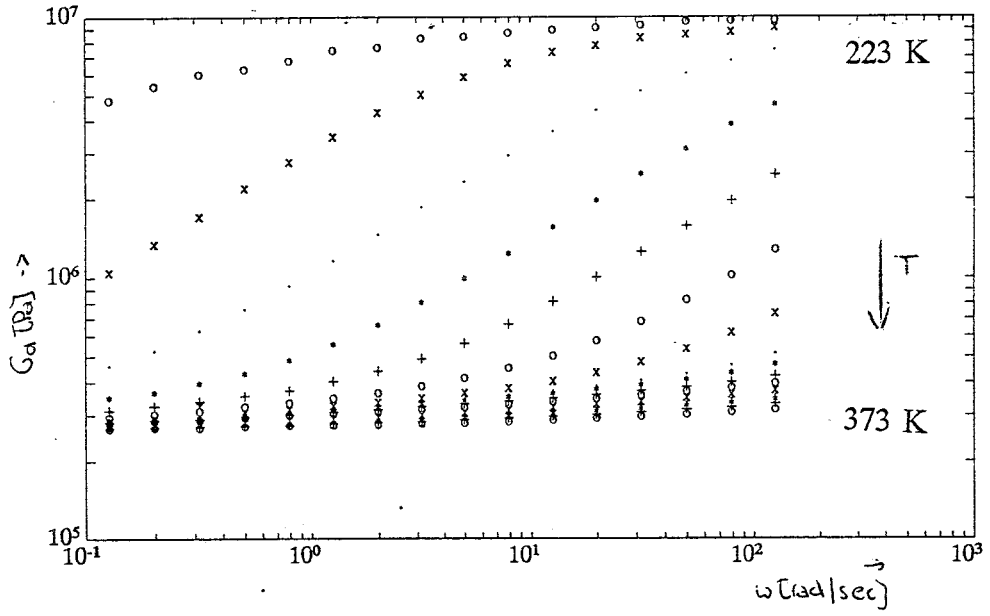

Figure 4.1: Butyl rubber, dynamic modulus versus angular frequency at temperatures from 223 K to 373 K.

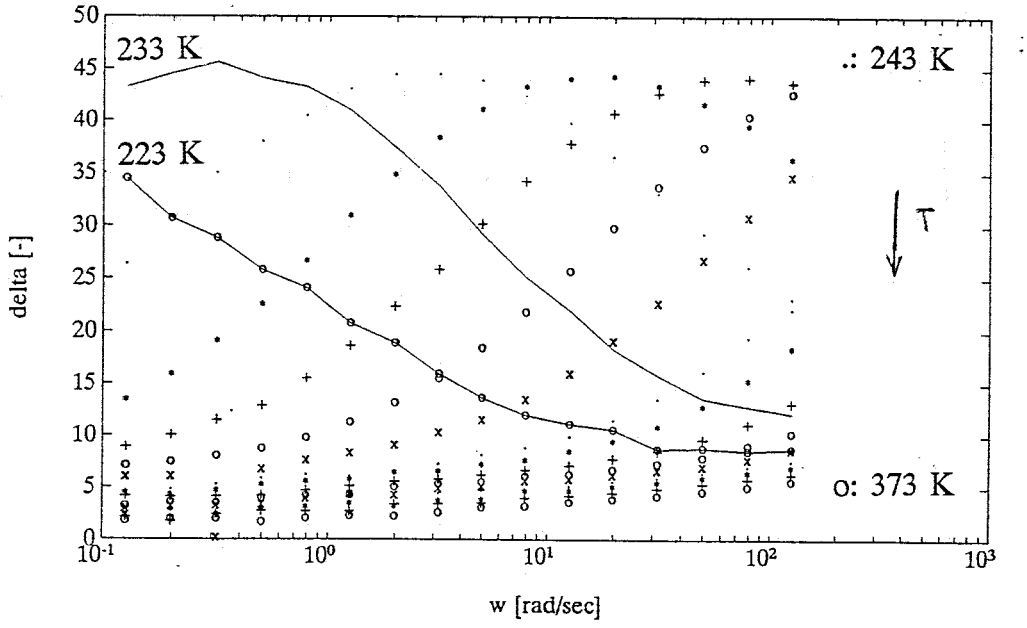

Figure 4.2: Butyl rubber, loss angle versus angular frequency at temperatures from 223 K to 373 K.

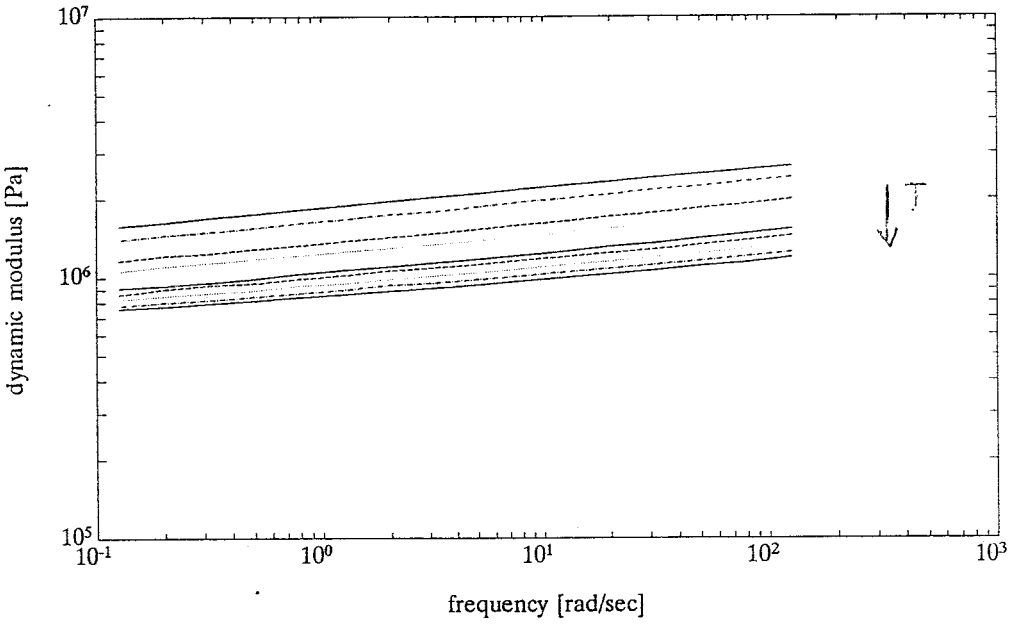

Figure 4.3: Silicone rubber, dynamic modulus versus angular frequency at temperatures from 293 K to 373 K.

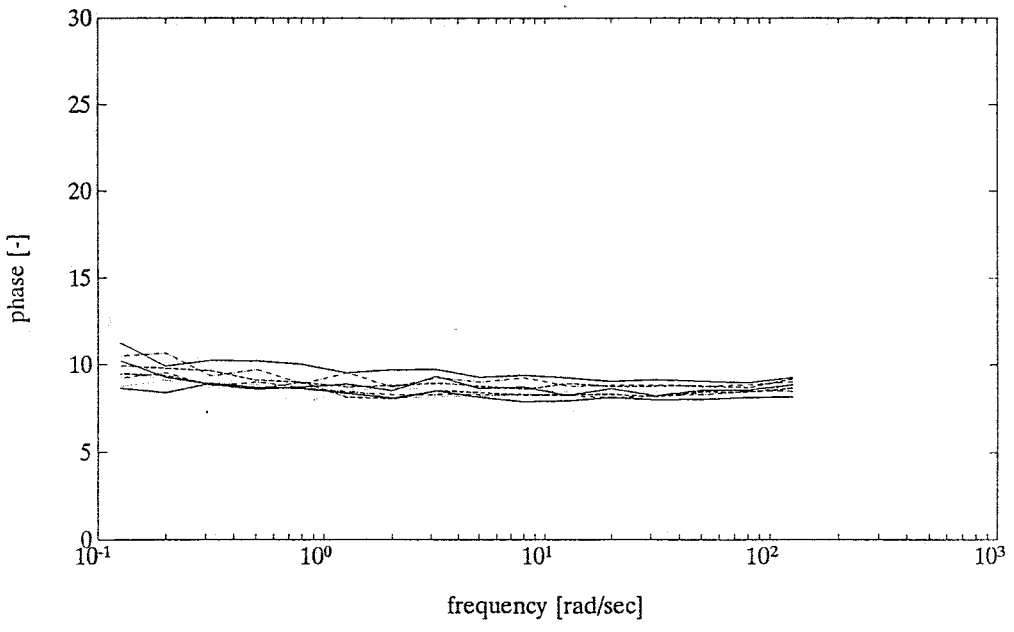

Figure 4.4: Silicone rubber, loss angle versus angular frequency at temperatures from 293 K to 373 K.

	Butyl rubber	Silicone rubber
c_1 [K]	6.21	8.40
c_2 [K]	144.9	107.2
T_0 [K]	296.3	313.6

Table 4.1: WLF parameters

in this way to shift the $|G^*(\log\omega)|$ curves. After which the vertical shift factors b_T can be deduced. This procedure guarantees the best values of a_T and b_T, since a_T is determined completely independent of b_T [41]. This procedure is adopted for butyl rubber and the result is shown in figure 4.5. The reference temperature T_0 is 293 K. For silicone rubber this procedure could not be used as the $\delta(\log\omega)$ curves at different temperatures overlap completely. Thus the horizontal shift-factors are determined with the use of the $|G^*(\log\omega)|$ curves. No additional vertical shift factors are determined. The master curve is obtained at a reference temperature of 313 K and is shown in figure 4.6.

The horizontal shift-factor a_T can be modelled by the WLF-equation (see appendix H):

$$\log a_T = \frac{-c_1(T - T_0)}{c_2 + (T - T_0)} \tag{4.8}$$

where c_1 and c_2 are constants obtained by fitting on the data. The results are shown in figures 4.7 and 4.8 and summarized in table 4.1.

4.4 Modelling

In the range of small deformations, the relation between the stress and strain can be described by a constitutive equation of the form [4]:

$$\boldsymbol{\tau}(t) = \int_{-\infty}^{t} G(t - t')\,\dot{\boldsymbol{\gamma}}(t')\,dt' \tag{4.9}$$

where $\boldsymbol{\tau}$ is the stress tensor.
$\dot{\boldsymbol{\gamma}}$ is the strain rate tensor.
$G(t)$ is the linear relaxation modulus.

The expression for the relaxation modulus G(t) that corresponds to multi-mode Maxwell behaviour is given by [14]:

$$G(t) = G_e + \sum_{i=1}^{N} g_i \exp(\frac{-t}{\theta_i}) \tag{4.10}$$

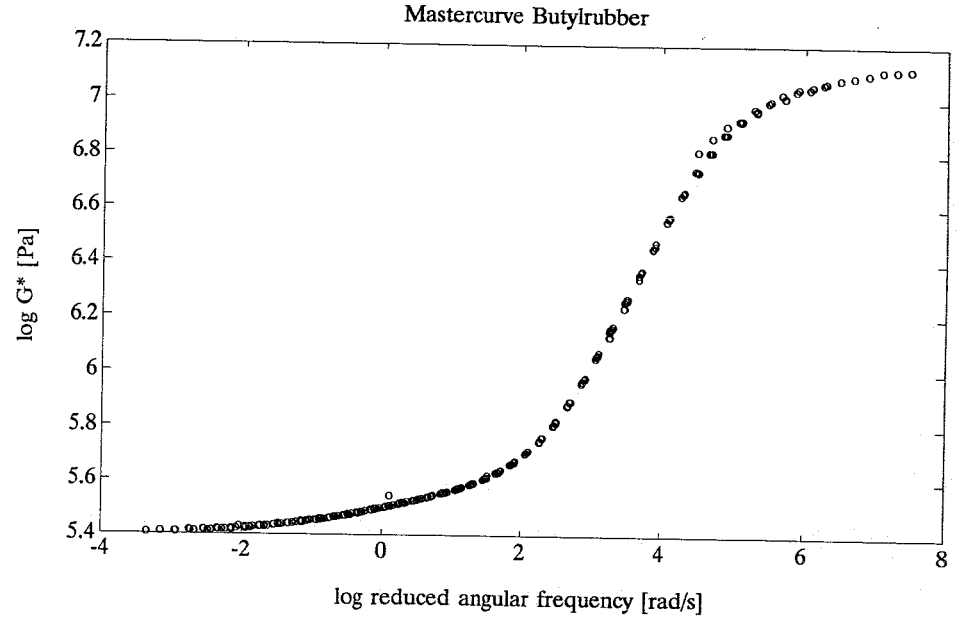

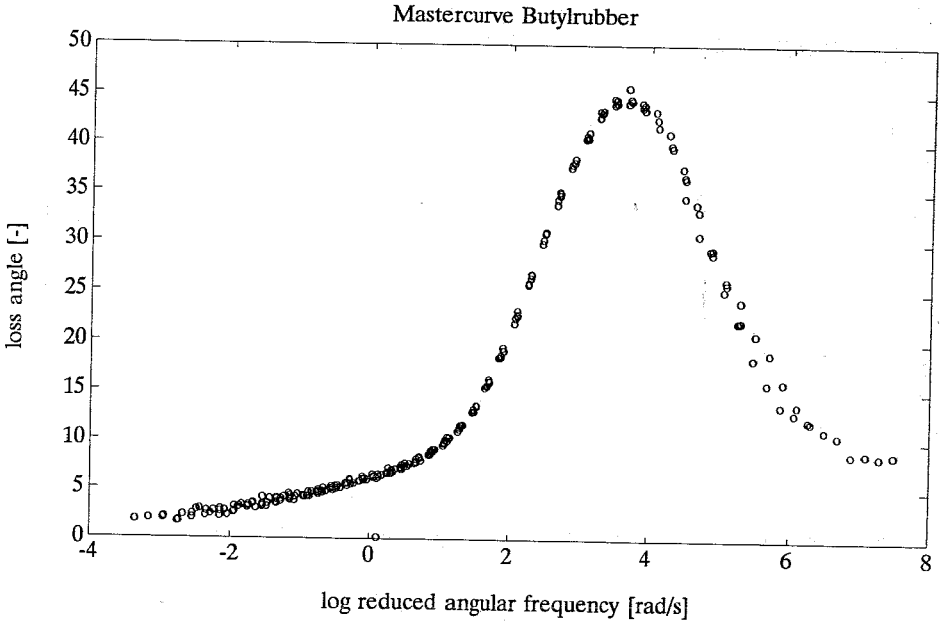

Figure 4.5: Butyl rubber, master curves, reference temperature 296.3 K.

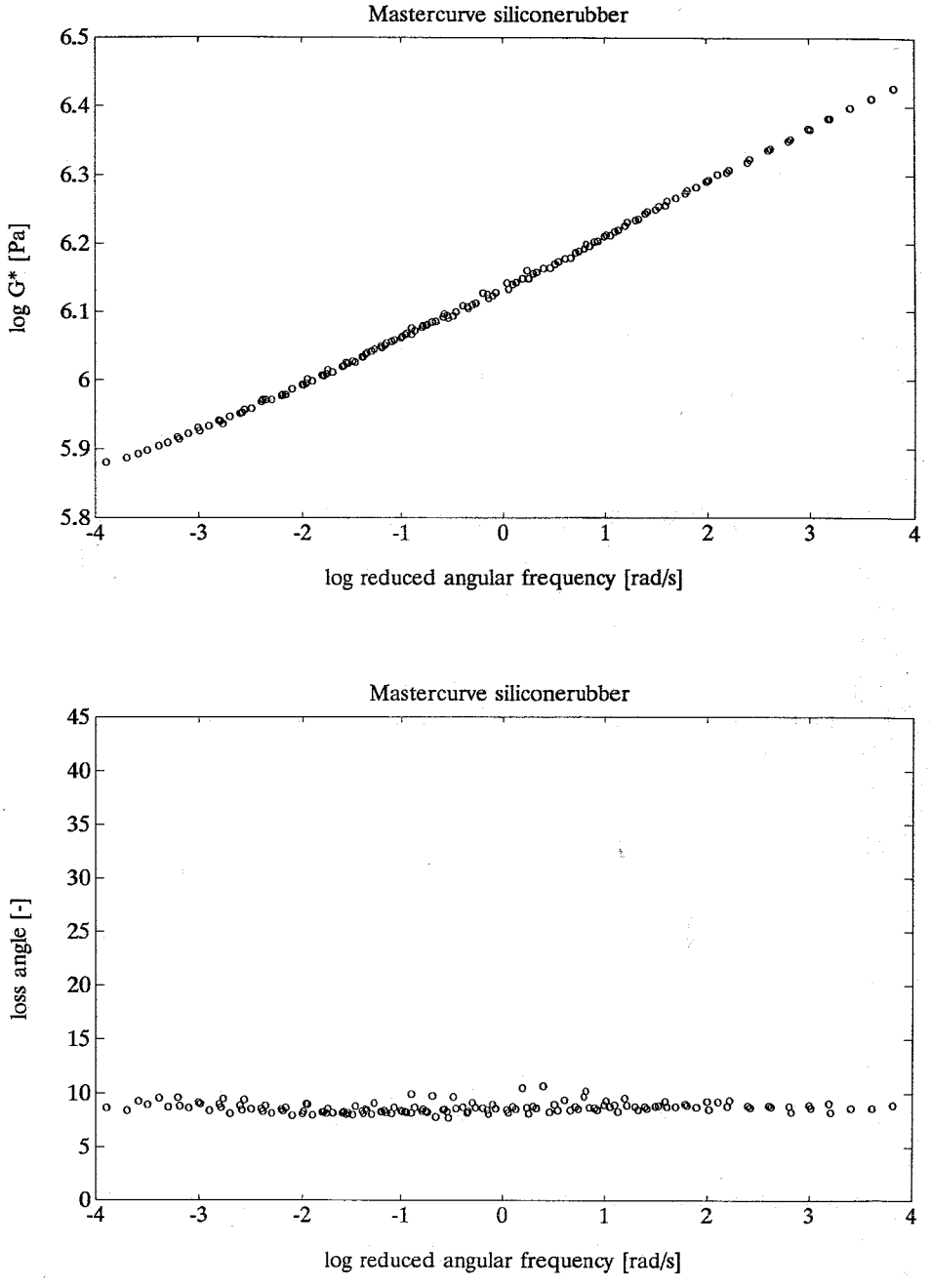

Figure 4.6: Silicone rubber, master curves, reference temperature 313 K.

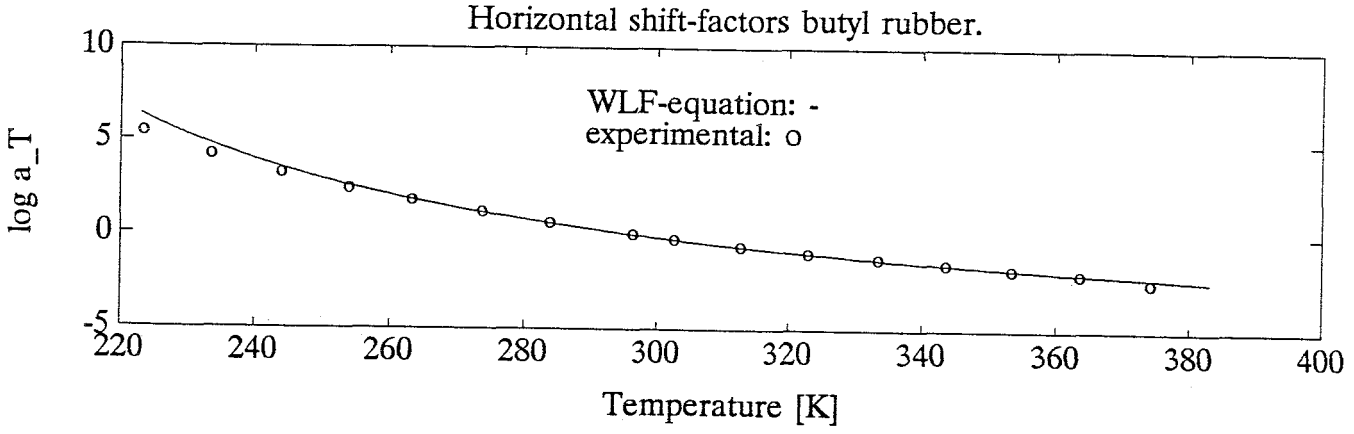

Figure 4.7: Butyl rubber, horizontal shift factor versus temperature (experimental: o, WLF-equation: -)

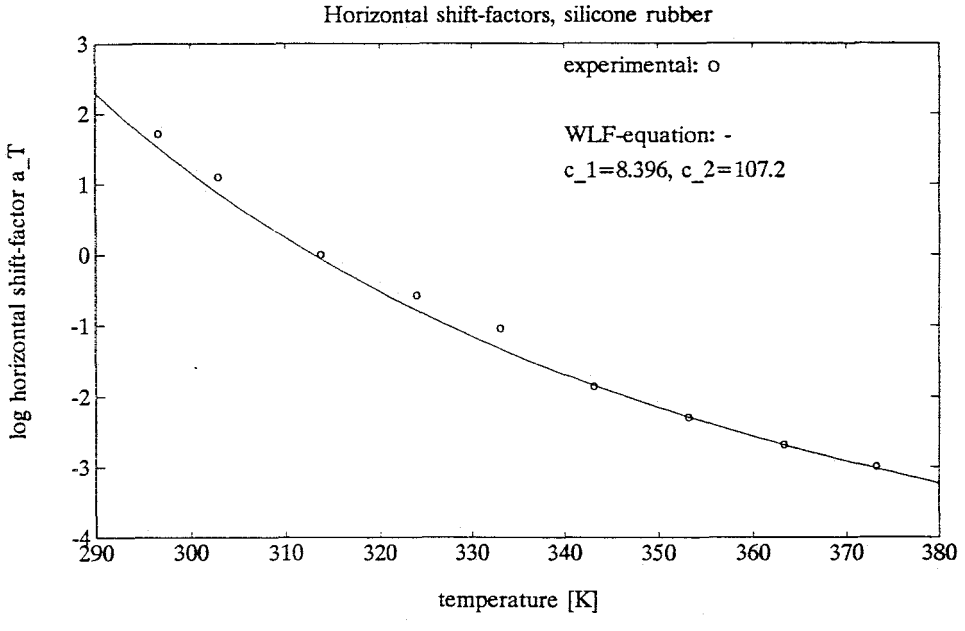

Figure 4.8: Silicone rubber, horizontal shift factor versus temperature (experimenal: o, WLF-equation: -)

The N relaxation modes are defined by their relaxation strengths g_i ($g_i = \frac{\eta_i}{\theta_i}$) and their relaxation times θ_i. The equilibrium modulus G_e is added to allow for a discrete distribution to the spectrum with $\theta_i = \infty$, for viscoelastic solids; for viscoelastic liquids (uncross-linked polymers), $G_e = 0$. In appendix I an expression for the dynamic moduli is derived:

$$G'(\omega) = G_e + \sum_{i=1}^{N} g_i \frac{(\omega\theta_i)^2}{1 + (\omega\theta_i)^2} \tag{4.11}$$

$$G''(\omega) = \sum_{i=1}^{N} g_i \frac{(\omega\theta_i)}{1 + (\omega\theta_i)^2} \tag{4.12}$$

The dynamic moduli (G', G'') have to be converted from the frequency to the time domain, in order to obtain the relaxation time spectrum G(t). Three methods of conversion are found in literature. The first method uses a Fourier transformation [4], the second method utilizes emperical correlations which are successful for a wide class of materials [14], and in the third method the parameters of a discrete relaxation spectrum are found by fitting equations 4.11 and 4.12 to the measured G', G'' data. The coefficients g_i and the relaxation times θ_i are determined such that the average square deviation between the predicted G', G'' data and the measured G', G'' data is minimum:

$$\min_{g_i,\theta_i} \sum_{j=1}^{m} [(\frac{G'(\omega_j)}{G'_m(\omega_j)} - 1)^2 + (\frac{G''(\omega_j)}{G''_m(\omega_j)} - 1)^2] \tag{4.13}$$

G'_m and G''_m are measured data at m frequencies ω_j, and G', G'' are calculated from equations 4.11 and 4.12.

The multi-mode Maxwell model is fitted on the mastercurves of butyl and silicone rubber. For both materials one fit is made with equilibrium modulus and one without. The results are listed in tables 4.2 and 4.3, and the fits are shown in figures 4.9 and 4.10. It can be readily seen that the best fit is obtained with use of an equilibrium modulus. The contribution of the different modes (with use of an equilibrium modulus) to the shear storage modulus and the loss modulus is plotted in figures 4.11 and 4.12

4.5 Model verification

In order to evaluate the use of the multi-mode Maxwell model with the coefficients determined in the previous section, predictions of the isochronal stress-strain curves have been compared with experimental data. In the previous chapter the stress

Maxwell fit at butyl rubber				
G_e	2.44e+5		-	
mode-no.	g_i	θ_i	g_i	θ_i
i=1	1.18e+4	2.24e+3	2.63e+5	2.24e+3
i=2	8.07e+3	2.31e+2	1.39e+4	2.38e+1
i=3	1.74e+4	2.38e+1	3.74e+4	2.45
i=4	3.27e+4	2.46	3.66e+4	3.70e-1
i=5	3.73e+4	2.53e-1	7.64e+4	4.42e-2
i=6	7.59e+4	2.61e-2	2.30e+5	4.38e-3
i=7	2.30e+5	2.69e-3	1.27e+6	3.46e-4
i=8	1.27e+6	2.78e-4	5.42e+6	3.04e-5
i=9	5.42e+6	2.86e-5	3.88e+6	2.99e-6
i=10	3.88e+6	2.95e-6	1.38e+6	6.96e-7
i=11	1.38e+6	3.04e-7	2.98e+6	7.34e-8
i=12	2.98e+6	3.13e-8	-	
E	1.83		4.44e+2	

Table 4.2: Linear viscoelastic parameters for butyl rubber.

Maxwell fit at silicone rubber				
G_e	5.99e+5		-	
mode-no.	g_i	θ_i	g_i	θ_i
i=1	1.62e+5	7.92e+3	8.25e+5	2.66e+4
i=2	1.03e+5	1.10e+3	1.73e+5	2.38e+2
i=3	1.41e+5	1.53e+2	1.57e+5	3.70e+1
i=4	1.54e+5	2.13e+1	1.82e+5	5.81
i=5	1.79e+5	2.96	2.12e+5	8.68e-1
i=6	2.11e+5	4.11e-1	2.31e+5	1.42e-1
i=7	2.31e+5	5.71e-2	3.07e+5	1.86e-2
i=8	3.07e+5	7.94e-3	2.63e+5	3.15e-3
i=9	2.62e+5	1.10e-3	6.45e+5	3.02e-4
i=10	6.45e+5	1.53e-4	-	-
E	0.739		2.01	

Table 4.3: Linear viscoelastic parameters for silicone rubber.

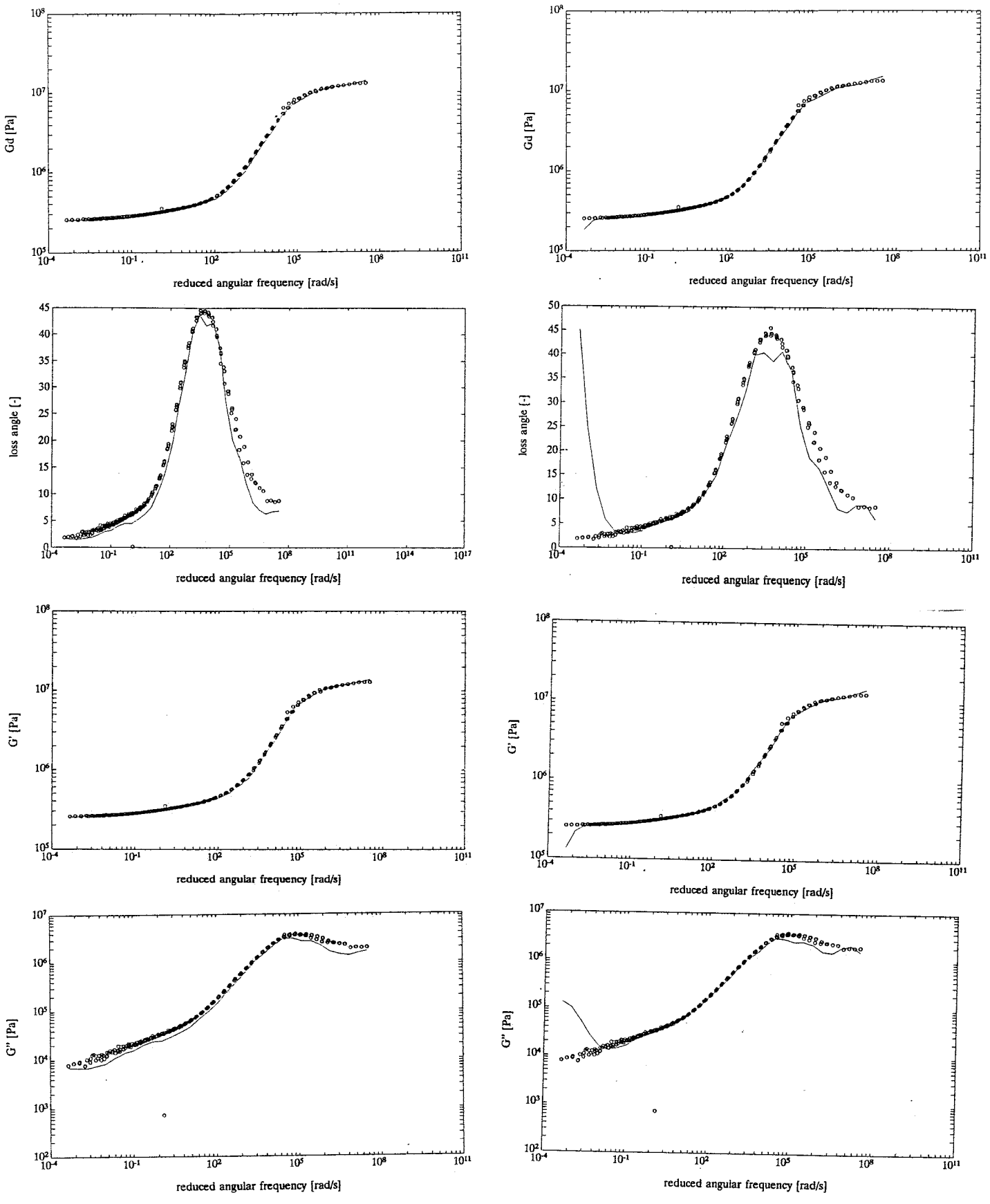

Figure 4.9: Maxwell fit at the viscoelastic functions of Butyl rubber, (experimental: o, fit: -). Left plots: with equilibrium modulus; right plots: without equilibrium modulus.

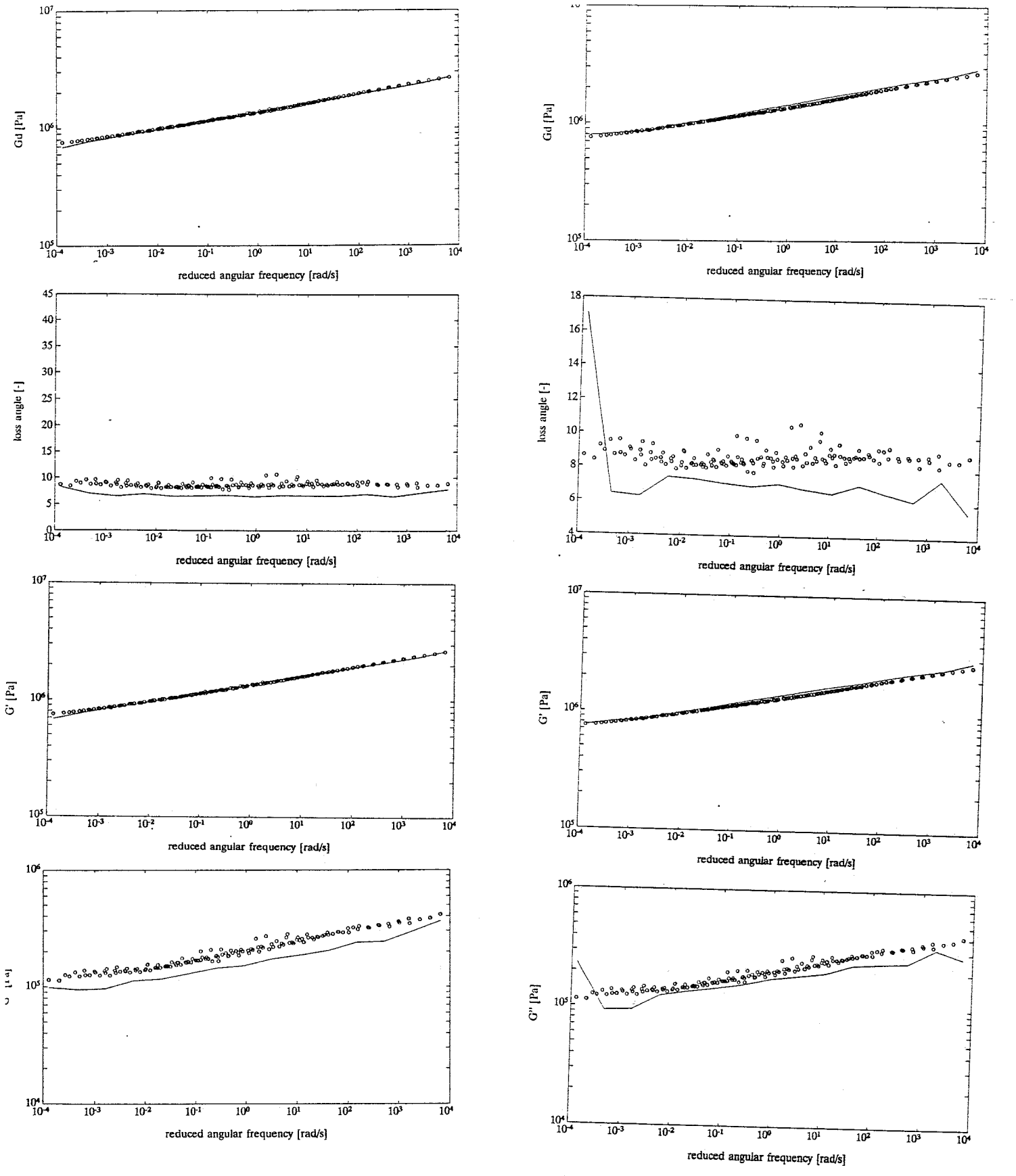

Figure 4.10: Maxwell fit at the viscoelastic functions of Silicone rubber (experimental:o, fit: -). Left plots: with equilibrium modulus; right plots: without equilibrium modulus.

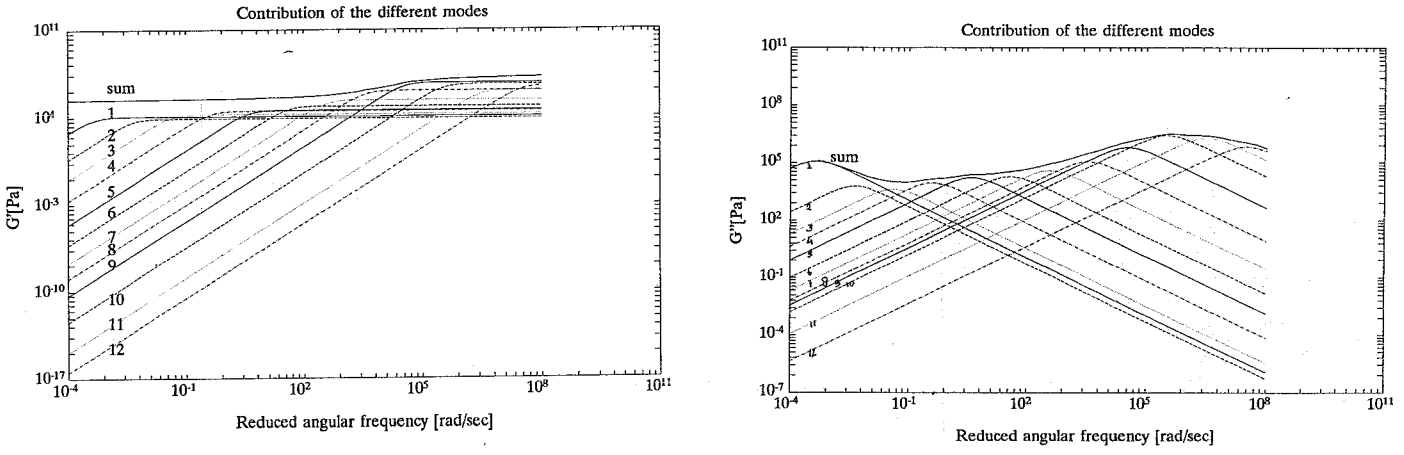

Figure 4.11: Contribution of the different modes, Butyl rubber

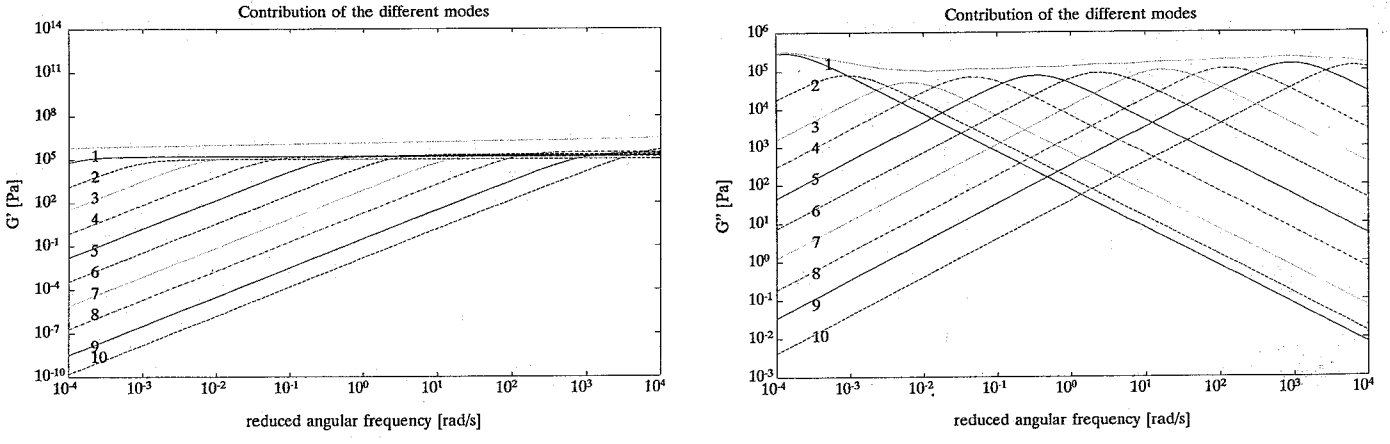

Figure 4.12: Contribution of the different modes, Silicone rubber

relaxation function in uniaxial tension of the multi-mode Maxwell model has been derived, and is given by:

$$\sigma_{11} = \sum_{i=1}^{n} c_i \exp \frac{-t}{\theta_i} \tag{4.14}$$

where c_i equals $3g_i$ due to the assumption of incompressibility. Thus the isochronal stress-strain curve in uniaxial tension is given by:

$$\sigma_{11} = \left\{ \sum_{i=1}^{n} 3g_i \exp \frac{-t}{\theta_i} \right\} \epsilon \tag{4.15}$$

The coefficients from tables 4.2 are substituted in the above equation. The result is compared with experimental data from stress relaxation measurements (see Chapter 3.) and plotted in figure 4.13 . It can be seen that the model predictions, with use of an equilibrium modulus, match well with the experimental data for Butyl rubber. As to be expected the model predictions without an equilibrium modelus do not match with the experimental results. The material constants for silicone rubber were determined at a reference temperature of 40 ^{o}C, however the stress relaxation experiments were conducted at 20 ^{o}C. The material constants are therefore transformed to 20 ^{o}C, with use of the experimentally determined shift-factor a_T. In figure 4.14 the model prediction is compared with the isochronal stress-strain curve. The results do not give a good agreement. Possible explanations are:

- The sample to sample variation.
- Because the silicone rubbers were vulcanized on the aluminium discs, used in the shear experiments differences in crosslink-density can occur, which results in a different shear modulus. Moreover the silicone rubbers, used in the stress-relaxation experiments are not completely vulcanized. This is based on the observation that the silicone rubbers are sticky, which suggests that the rubber still contains some oil [44].
- Crystallinity.

Preleminary DMTA and DSC experiments (see appendix J) show strange endothermal effects and indicate that the silicone rubber is a semi-crystalline material. This makes its application for dampers doubtfull because due to the crystallization, the mechanical behaviour is not reproducible. Further investigations of this phenomenon are beyond the scope of this work.

4.6 Non-linearity in shear

In order to evaluate the non-linear behaviour of the rubber compounds in shear, dynamic measurements with a small amplitude ($\gamma_0 = 1.5\%$) are conducted at a

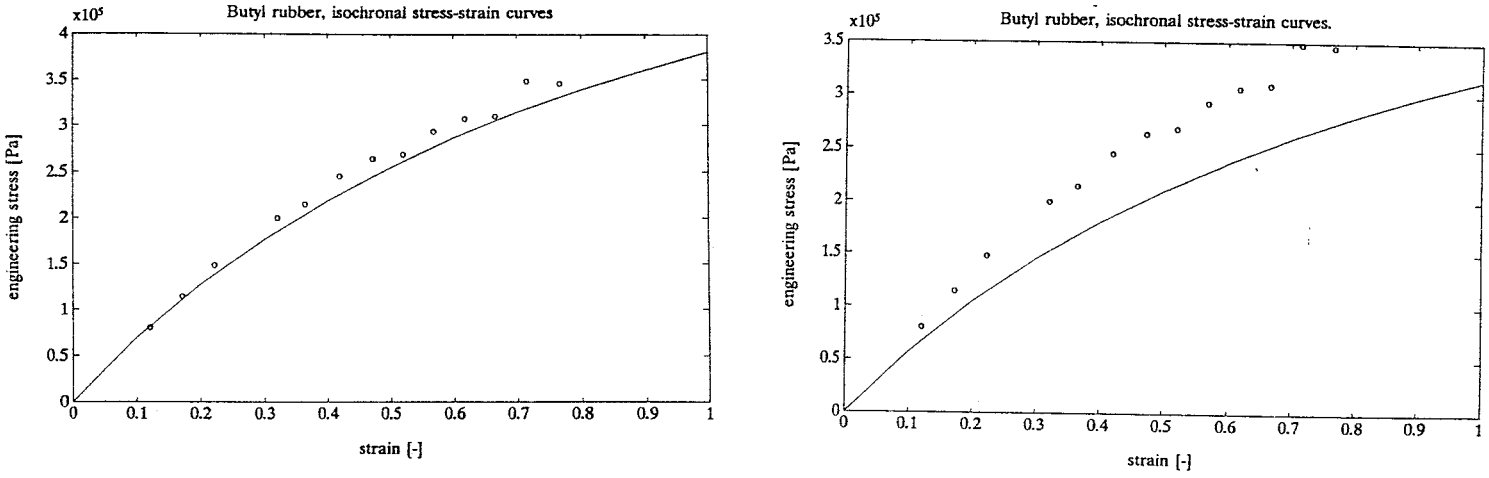

Figure 4.13: Comparisson of isochronal stress-strain curves for butyl rubber (experimental: o Maxwell model: -, with equilibrium modulus: left plot, without equilibrium modulus: right plot)

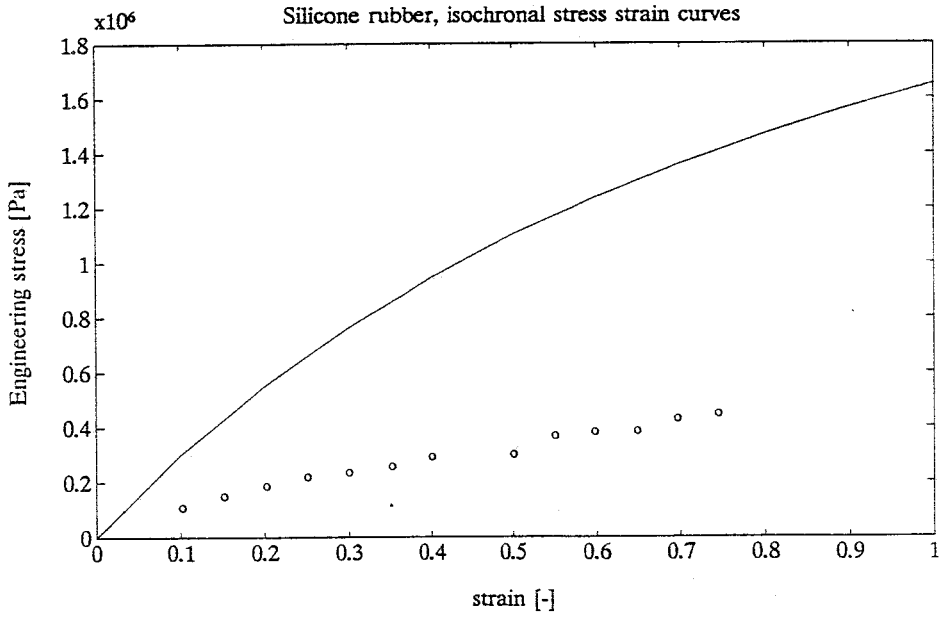

Figure 4.14: Comparisson of isochronal stress-strain curves for silicone rubber (experimental: o Maxwell model with equilibrium modulus: -

frequency of 10 Hz, with the RDS2. The dynamic moduli G' and G'' are obtained for different fixed shear strain levels. The measurements are repeated 3 times and the average values are computed. With use of these dynamic moduli, the stresses can be calculated.

For butyl rubber, the results from three different samples, are shown in figure 4.15. It can be readily seen that for the considered strain domain, the stress linearly depends on the strain. The sample to sample variability is smaller than 12 %. The average dynamic modulus $|G^*|$ equals to 3.7e+5 Pa. From the isochronal stress-strain curve in uniaxial tension (See chapter 3) the Young's modulus E is estimated to equal to 9e+5. Because rubbery materials are virtually incompressible in bulk, the value Poisson's ratio is close to 0.5. E is therefore given by $3|G^*|$ to good approximation. There is approximately 23 % deviation between the results obtained in uniaxal extension and the results obtained in shear. This can be explained by the sample to sample variation (The samples used in shear and the ones used in uniaxial tension are from a different batch) and the difficulty to define the zero point in uniaxial tension.

For silicone rubber,new samples were prepared, because with the original cone-and-plate samples strain levels could be reached untill at most 15 %. After preparation, the samples were turned on a lathe untill they reached a diameter of 10 mm. The results for three different samples are shown in figure 4.16. Untill a strain level of about 80 % the stress is approximately linearly dependend on the strain. The sample to sample variation is within 20 %. Comparison of three times the average initial dynamic modulus ($3|G^*|$ equals 3.385e+6) with the initial modulus of the isochronal stress strain curve in uniaxial extension (estimated to equal 1.1e+6) shows a deviation of approximately 210 %. This large difference is probably due to the same reason as the cause of the difference between the model predictions for silicone rubber in a stress relaxation experiment and the experimental data (see previous section).

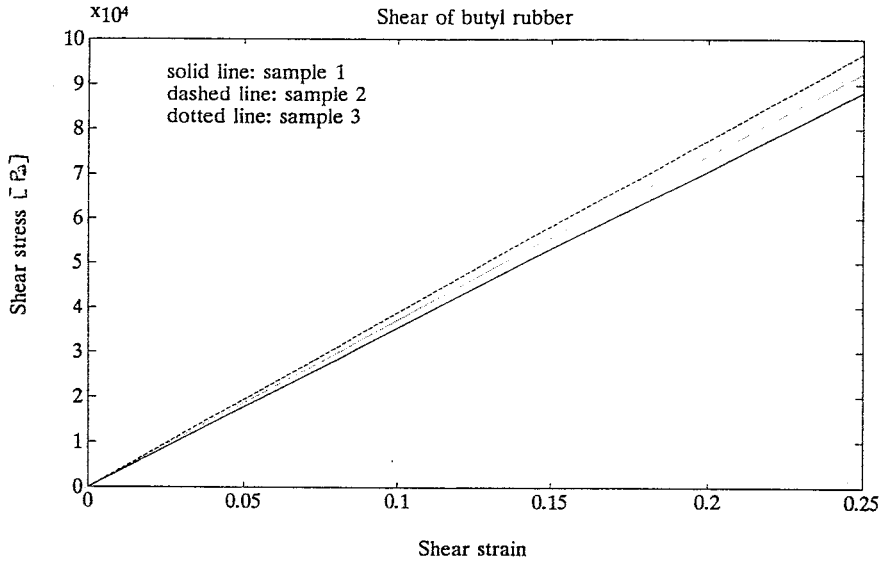

Figure 4.15: Shear of butyl rubber

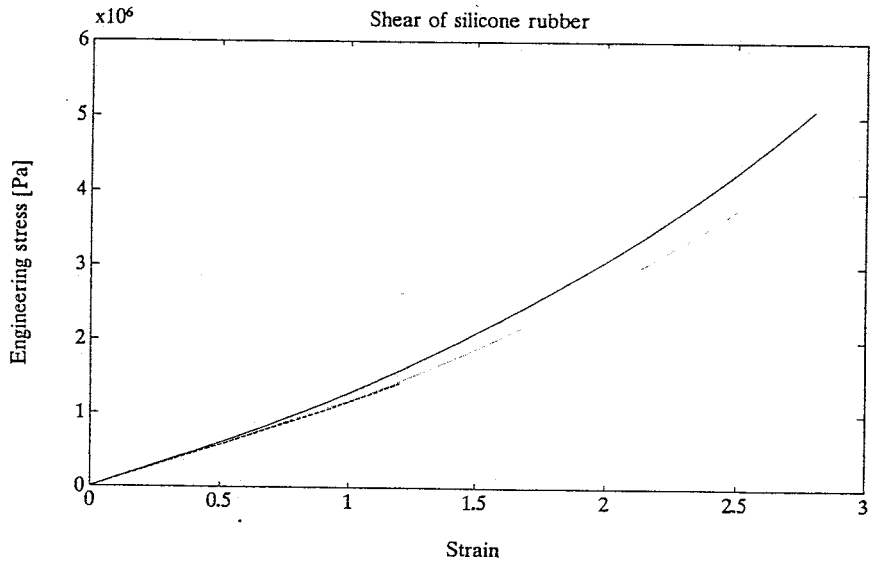

Figure 4.16: Shear of silicone rubber

Chapter 5

Results of numerical simulations

5.1 Introduction

In this work interest is focused on design requirements for rubber dampers. Hysteresis curves and transfer functions are measures of the amount of damping exhibited by a material. In the following sections the results of numerical simulations of hysteresis curves and transfer functions are presented.

5.2 Hysteresis curves of butyl and silicone rubber

The stresses observed during the return of a stretched rubber to an unstrained state are less than the corresponding stresses during the extension. This difference is related to the loss of energy and therefore is a measurement for the amount of damping of the material. So, the larger this difference, the larger the amount of damping of the material.

With the program PCMatlab hysteresis curves of different rate-type constitutive equations are obtained. In reference [6] these curves for various models can be found. As noted in appendix B, from these models the multi-mode Maxwell model describes the Mullins effect best.

Because geometry effects are not included in the above mentioned calculations, the multi-mode Maxwell model has been implemented in the finite element code SEPRAN. For different geometries hysteresis curves are computed. The material parameters used in these calculations were obtained in chapter 4 for both a butyl and a silicone rubber. It should be noted that the parameters for silicone rubber were obtained at a reference temperature of 40 $^{\circ}C$. Therefore these parameters were transformed to a reference temperature of 20 $^{\circ}C$, with use of the experimentally determined shift factor a_T.

The hysteresis curves in uniaxial tension were simulated on a rectangular bar.

The results are shown in appendix K Comparisson with experimental results, figure K.1, shows that the multi-mode Maxwell model is able to describe the Mullins-effect qualitatively. However the degree of damping, predicted by the Maxwell model is too low. Moreover the Maxwell model predicts too high stresses for strains larger than 30 %. It should be noted that the butyl rubber on which the material data was obtained and the rubber used in the hysteresis experiments originate from a different batch. Furthermore the experiments were conducted on rubber rings and the calculations were performed on bars. In reference [34] it can be seen that the area between the curves is smaller for hysteresis tests performed on bars than for the same test performed on rubber rings. Therefore it is strongly suggested that more hysteresis experiments should be conducted, in order to evaluate properly the predictive qualities of the multi-mode upperconvected Maxwell model. Comparison of figure K.1 with figure K.2 and of figure K.3 with figure K.4 shows that the tensile modulus increases with increasing strain-rate. This is in agreement with experimental data [34]. Moreover the silicone rubber exhibits more damping than the butyl rubber.

In order to evaluate the effects of geometry hysteresis curves in uniaxial pressure were conducted on blocks and on hollow pipes. The results are shown in appendix L. For the pipe strain-levels for approximatelly 20 % could be reached at most. Above 20 % the system matrix was singular. A possible explanation is bending of the side walls of the hollow pipe. This hypothesis is supported by the fact that for thicker walls higher strain-levels could be reached, and that if more elements are taken in the length of the pipe lower strain-levels were reached. An explanation is that a larger amount of elements gives a more accurate description of bending phenomena. When smaller displacement steps are taken, somewhat higher strain levels can be reached but the computation is stopped, because of convergence problems. In figure L.4 a typical force-deflection curve of a pipe is shown. Bifurcation occurs at the point where the pipe starts to bend. At this point the system matrix will be singular. Comparisson of the results of the hysteresis tests on pipes (untill strain levels of 20 %) with tests on cubes show no difference in the amount of energy dissipated by the material.

5.3 Transfer functions of butyl and silicone rubber

The performance of a damper is ussually given in terms of transmissibility. Transmissibility is defined as the ratio of the transmitted amplitude to the imposed amplitude of vibration or the ratio of the transmitted force to the externally imposed force. In a Bode plot the absolute value of the transmissibility and the phase are plotted against frequency. An effective damper should have a low natural frequency of vibration, a low transmissibility at resonance, and a transmissibility that decreases

rapidly with frequencies, at frequencies greater than the natural frequency.

In appendix M the transfer function of a Maxwell element is derived. The multi-mode Maxwell model is obtained by considering n Maxwell elements in parallel. With the program PCMatlab Bode diagrams of the transfer function can be plotted. This is done for both silicone and butyl rubber. The results are shown in appendix N. From figures N.1, N.2, N.3 and N.4 it can be seen that the performance of the dampers is better in shear than in uniaxial tension, because in shear the natural frequency of vibration is lower. Furthermore the silicone rubber exhibits better damping characteristics than the butyl rubber. In the spring constant k and the dashpot viscosity c, occuring in the transfer function, the sample area and the sample length are negotiated. Comparisson of figure reffig:BBode2 with figure N.5 and figure N.4 and figure N.6shows that a smaller ratio of the sample area to the sample length yields a better transmissibility.

As noted in chapter 2, it is possible to derive the transfer function of a prestressed material of arbitrary shape with the finite element package MARC. However numerical simulations showed that this option was not correctly implemented in MARC. In an uniaxial tensile test stresses occured not only in the direction of the tensile force but also in all the other directions. Just recently before printing this report, the MARC research analysis corporation implemented the correct version of Lianis' constitutive equation. The mistakes were concerned with the strain measure and the IBM-specific vectorized subroutine solver.

Chapter 6

Conclusions and Suggestions

This project has provided us with a better insight in the computation of the dynamic behaviour of rubber materials. In order to model the material behaviour of rubber, two constitutive equations have been considered: the multi-mode Maxwell model and Lianis' equation. The material parameters, occuring in these theories, have been determined for two types of rubber, namely a silicone and a butyl rubber. Numerical simulations were conducted in order to evaluate the predictive quality of the models concerning the damping properties of the material. The main conclusions obtained from this work, along with some suggestions for further research are summarized below.

- From stress relaxation measurements in uniaxial tension the isochronal stress-strain curve has been obtained. The degree of non-linearity is such that for both a silicone and a butyl rubber the multi-mode Maxwell model, two modes are sufficient, is able to describe this stress-strain behaviour, in the strain range of 0-70 %.

- From linear viscoelastic dynamic shear measurements the material parameters have been determined. With use of these material parameters the isochronal stress-strain curves of silicone and butyl rubber were predicted by the multi-mode Maxwell model. For butyl rubber the model predictions matched well with the experimental data. For silicone rubber, however, the results did not match. Instead of the tensile modulus being equal to three times the shear modulus, it was equal to the shear modulus. This is probably caused by the semi-crystallinity of the silicone rubber, as indicated by preleminary DMTA and DSC measurements.

- For butyl rubber the material behaviour in shear has been determined in the strain range of 0-25 %. In this range the material behaves linear. For silicone rubber shear data have been obtained in the strain range of 0-250 %. Untill approximatelly 80 % the material behaviour in shear is linear.

- The multi-mode Maxwell model is able to describe qualitatively the Mullins effect. In order to investigate the predictive quality of this model more accurately, more experimental data of hysteresis curves should be obtained.
- Numerical simulations in uniaxial tension showed that Lianis' constitutive equation was not correctly available in the finite element code MARC. In future the predictive quality of transfer functions, for different geometries, of Lianis' equation should be investigated. Eventually the equations of small strains superposed on large prestrains should be derived as a function of frequency from the multi-mode Maxwell model, followed by implementation in the finite element code SEPRAN.

References

[1] D.R. Axelrad. Mechanical models of relaxation phenomena. *Advan. Mol. Relaxation Processes*, 2:41-68, 1970.

[2] F.P.T. Baaijens. *A constitutive equation for compressible polymeric liquids.* Philips, internal report, 1987.

[3] F.P.T. Baaijens. *Applied computational mechanics.* University of Technology Eindhoven, march 1991

[4] M. Baumgaertel and H.H. Winter. Determination of discrete relaxation and retardation time spectra from dynamic mechanical data. *Rheol. Acta* 28:511-519, 1989.

[5] J.J.M. de Bever. *Three-dimensional finite element modelling and computer simulation of a viscoelastic rubber material.* WFW-report 91.027, Eindhoven maart 1991.

[6] J.J.M. de Bever. *Literature survey to the dynamic behaviour of rubber and rubberlike materials.* WFW-report 92.006, Eindhoven january 1992.

[7] W.A.M. Brekelmans. *Non-linear mechanics: numerical aspects* (in Dutch). CEM-course 1988-89, University of Technology Eindhoven.

[8] H.C. Booy and J.H.M. Palmen. Some aspects of linear and nonlinear viscoelastic behaviour of polymer melts in shear. *Rheol. Acta* 21:376-387, 1982.

[9] W.V. Chang, R. Bloch and N.W. Tschoegl. On the theory of viscoelastic behavior of soft polymers in moderately large deformations. *Rheol. Acta*, 15:367-378, 1976.

[10] W.V. Chang, R. Bloch and N.W. Tschoegl. The behavior of rubberlike materials in moderately large deformations. *Journal of Rheology*, 22:1-32, 1978.

[11] L. Douven. *Towards the computation of properties of injection moulded products: flow and thermally induced stresses in amorphous thermoplastics.* Ph.D.-thesis, Eindhoven 1991

[12] F.R. Eirich. *Science and technology of rubber.* Academic press, New York, 1978.

[13] A.C. Eringen. *Nonlinear theory of continuous media.* McGraw-Hill Book Company, Inc, 1962.

[14] J.D. Ferry. *Viscoelastic properties of polymers.* John Wiley & Sons, inc. New York, 1970.

[15] P.K. Freakley and A.R. Payne. *Theory and practice of engineering with rubber,* pages 24-32. Applied Science Publishers London, 1978.

[16] V.M. Geelen. *Literature study passive rubber dampers for outdoor CD-players* (in Dutch). Competence Centre Plastics, Philips internal report PHB-08K-013-335, 1991.

[17] L.E. Govaert. *Deformation behaviour of oriented polyethylene fibres.* PhD-thesis, Eindhoven 1990

[18] Personal communications with L.E. Govaert, University of Technology Eindhoven, 1992.

[19] G. Hamed. Free volume theory and the WLF equation. *Elastomerics.* January, 1988.

[20] J.A.C. Harwood, L.Mullins and A.R. Payne. Stress softening in natural rubber vulcanizates part II. Stress softening effects in pure gum and filler loaded rubbers. *Journal of polymer science,* 9:3011-3021, 1965.

[21] S.A. Kahn and R.G. Larson. Comparison of simple constitutive equations for polymer melts in shear and biaxial and uniaxial extension. *Journal of Rheology,*31: 207-234, 1987

[22] C.M. Kootwijk-Damman. *Reologie van LCP's met starre hoofdketens en flexibele zijketens.* CPM-TNO, nr. 691/'90 september 1990.

[23] R.G. Larson. *Constitutive equations for polymer melts and solutions.* Butterworhts, Boston 1988.

[24] A.I. Leonov. Nonequilibrium thermodynamcis and rheology of viscoelastic polymer media. *Rheologica acta,* 15: 85-98, 1976.

[25] A.I. Leonov and A.N. Prokunin. An improved simple version of a non-linear theory of elasto-viscous polymer media. *Rheologica acta,* 19: 393-403.

[26] A.I. Leonov. On a class of constitutive equations for viscoelastic liquids. *Journal of Non-Newtonian Fluid Mechanics,* 25: 1-59, 1987.

[27] G. Lianis. Small deformations superposed on an initial large deformation in viscoelastic bodies. *Proc. Fourth Int. Congress on Rheology.* pt 2, Interscience, New York 1963.

[28] G. Lianis Problems of small strains superposed on finite deformation in viscoelastic solids. *Proc. Fourth Int. Congress on Rheology, part 2*, pages 104-119 1965

[29] F.J. Lockett. *Nonlinear viscoelastic solids.* Academic press London, 1972.

[30] *Marc user manuals, volumes A,B,C,D and E* version K3. Marc analysis research Corporation, 1988.

[31] K.N. Morman and J.C. Nagtegaal Finite element analysis of sinusoidal small-amplitude vibrations in deformed viscoelastic solids. Part 1: theoretical development. *Int. Journal for numerical methods in engineering* 19:1079-1103, 1983.

[32] L.Mullins and N.R. Tobin. Stress softening in rubber vulcanizates part I. Use of a strain amplificaton factor to describe the elastic behaviour of filler reinforced vulcanized rubber. *Journal of polymer science*, 9:2993-3009, 1965.

[33] R.W Ogden. Large deformation isotropic elasticity - on the correlation of theory and experiment for incompressible rubberlike solids. *Proc. R. Soc. Lond. A*, 326: 565-584, 1972.

[34] F.N. Paridaans *Mechanical characterization of butyl rubber K1043 and sil.H40 rubber for suspensions inside portable CD-players.* Philips technical note PHR-08k-304-103, 1991

[35] S.T.J. Peng and R.F. Landel. Stored energy function and compressibility of compressible rubberlike materials under large strain. *J. of applied Physics*, 46:2599-2604, 1975.

[36] N. Phan Thien and R.I. Tanner. A new constitutive equation derived from network theory. *J. of Non Newtonian Fluid Mechanics*, 2: 253-365, 1977.

[37] A.C. Pipkin and T.G. Rogers. A non-linear integral representation for viscoelastic behaviour. *J. Mech. Phys. Solids*, 16: 59-72, 1968.

[38] R.S. Rivlin and J.L. Ericksen. Stress-deformation relations for isotropic materials. *Journal of Rational Mechanics and Analysis*, 4:325-425, 1955.

[39] C.M. Roland The Mullins effect in crosslinked rubber. *Journal of Rheology*,659-670, 1989

[40] R.A. Schapery. An engineering theory of nonlinear viscoelasticity with applications. *Int. J. Solids Structure*, 2:407-425.

[41] B.J.R. Scholtens. Linear thermoviscoelasticity and characterization of noncrystalline EPDM rubber networks. *Journal of polymer science.* 22:317-344, 1984.

[42] Sepran manuals. *User's Manual, Progammers Guide and Standard Problems.* Ingenieursbureau SEPRA, Leidschendam 1984.

[43] P.R. Soskey and H.H. Winter. Large step shear strain experiments with parallel disk rotational rheometers. *Journal of Rheology.* 28:625-645, 1984.

[44] Personal communications with A. Spoelstra, University of Technology Eindhoven.

[45] L.R.G. Treloar. *The physics of rubber elasticity*, Third edition. Claredon Press Oxford, 1975.

[46] K.C. Valanis and R.F. Landel The strain energy function of a hyperelastic material in terms of the extension ratios. *J. of applied Physics*, 38:2997-3002, 1967.

[47] F.E. Veldpaus. *Inleiding continuumsmechanica* Collegedictaat 4612, University of Technology, Eindhoven 1984.

[48] J.L. White and A.B. Metzner. Development of constitutive equations for polymeric melts and solutions. *Journal of Applied Polymer Science*, 7:1867-1889, 1963.

Appendix A

Basic principles of continuum mechanics

A.1 Introduction

In this appendix, the basic principles of continuum mechanics are summarized. The rubber material is considered as a continuum. The assumption is made that the temperature is not of relevant importance during the deformation. The deformation of a continuum can then be described completely when the position vector of the material points $\vec{x}$, the Cauchy stress tensor $\boldsymbol{\sigma}$ and the density ρ are known. The position vector has three components, the Cauchy stress tensor has nine and the density is a scalar, in a three-dimensional problem. Consequently there are thirteen unknowns. The deformation process has to satisfy three local balance laws, which result in a set of seven equations. They are presented in section A.3. To create a solvable set of equations, six extra equations have to be formulated, which are called the constitutive relations. They are characteristic for the used material and describe the behaviour of that material under influence of external forces. A number of constitutive principles, derived form physics, to which the constitutive equations have to obbey are summarized in section A.4. First in section A.2 a short introduction is given into the kinematics of a continuum.

A.2 Kinematics of a continuum

A continuum is considered to exit of a set of material points. Each of these material points are identified with a set of unchanging parameters, the so-called material coordinates. These material coordinates are denoted by a column $\underset{\sim}{\xi}$. The current position vector of a point P in the continuum, denoted by $\vec{x} = \vec{X}(\underset{\sim}{\xi}, t)$ is a function of these material coordinates $\underset{\sim}{\xi}$ and of the time t. $\vec{x}(\underset{\sim}{\xi}, t)$ is assumed to be continuous and differentiable with respect to both $\underset{\sim}{\xi}$ and t. The current configuration Ω is

the set of current position vectors of all material points of the continuum. The deformation of a continuum is described with respect to its reference configuration Ω_0. This is a configuration at a chosen time t_0. A so-called Lagrangian description is obtained if the initial undeformed state is chosen as a reference configuration.

The relation between a material point in the current configuration and that point in the reference configuration is described by the deformation tensor $\mathbf{F}$. $\mathbf{F}$ is defined as:

$$\mathbf{F} = (\vec{\nabla}_0 \vec{x})^c \quad ; \quad d\vec{x} = \mathbf{F} \cdot d\vec{x}_0 \tag{A.1}$$

where: $\vec{\nabla}_0$ is the gradient operator with respect to the reference configuration.
$\vec{x}$ is the position vector in the current configuration.
$d\vec{x}$is the distance vector between two neighbouring material points P and Q in the current configuration.
$d\vec{x}_0$is the distance vector between these material points in the reference configuration.

The determinant of this deformation tensor is equal to the ratio of the volume of the body in the current configuration and the volume in the reference configuration. It can easily be shown that for an incompresible material $\det(\mathbf{F}) = J = 1$ (no volume change).

The polar decomposition theorem allows $\mathbf{F}$ to be written in either of the unique forms:

$$\mathbf{F} = \mathbf{R} \cdot \mathbf{U} = \mathbf{V} \cdot \mathbf{R} \tag{A.2}$$

where $\mathbf{R}$ is an orthogonal matrix and $\mathbf{U}$ and $\mathbf{V}$ denote positive definite symmetric matrices. The physical interpretation of equation A.2 is that the deformation can be considered as a rigid rotation $\mathbf{R}$ which is either preceded by a pure stretch $\mathbf{U}$ or followed by a pure stretch $\mathbf{V}$. More convenient strain measures are the right and left Cauchy Green strain tensors $\mathbf{C}$ and $\mathbf{B}$ respectively, defined by:

$$\mathbf{C} = \mathbf{F}^c \cdot \mathbf{F} = \mathbf{U}^c \cdot \mathbf{R}^c \cdot \mathbf{R} \cdot \mathbf{U} = \mathbf{U}^2 \tag{A.3}$$

$$\mathbf{B} = \mathbf{F} \cdot \mathbf{F}^c = \mathbf{V} \cdot \mathbf{R} \cdot \mathbf{R}^c \cdot \mathbf{V}^c = \mathbf{V}^2 \tag{A.4}$$

The invariants of $\mathbf{C}$ and $\mathbf{B}$ which will be used extensively in later sections, are equal to eachother and are defined by:

$$I_1 = \mathrm{tr}(\mathbf{C}) \tag{A.5}$$

$$I_2 = \frac{1}{2}\left[\mathrm{tr}^2(\mathbf{C}) - \mathrm{tr}(\mathbf{C}^2)\right] \tag{A.6}$$

$$I_3 = \det(\mathbf{C}) \tag{A.7}$$

Another convenient strain measure is the Green-Lagrange strain tensor, defined by:

$$\mathbf{E} = \frac{1}{2}(\mathbf{C} - \mathbf{I}) = \frac{1}{2}(\mathbf{F}^c \cdot \mathbf{F} - \mathbf{I}) \tag{A.8}$$

where $\mathbf{I}$ is the unity tensor. By considering the displacement vector $\vec{u}$, given by:

$$\vec{u} = \vec{x} - \vec{x}_0 \tag{A.9}$$

and application of equation A.1 it can be shown that:

$$\mathbf{E} = \boldsymbol{\epsilon} + \frac{1}{2}(\vec{\nabla}_0 \vec{u}) \cdot (\vec{\nabla}_0 \vec{u})^c \tag{A.10}$$

where $\boldsymbol{\epsilon}$ is the classical linear strain tensor defined as:

$$\boldsymbol{\epsilon} = \frac{1}{2}\{(\vec{\nabla}_0 \vec{u}) + (\vec{\nabla}_0 \vec{u})^c\} \tag{A.11}$$

Thus, when the displacement gradients are small, $\mathbf{E}$ reduces to the classical linear strain measure $\boldsymbol{\epsilon}$.

The velocity gradient tensor $\mathbf{L}$ is defined as:

$$\mathbf{L} = (\vec{\nabla}\vec{v})^c = \dot{\mathbf{F}} \cdot \mathbf{F}^{-1} \tag{A.12}$$

$\mathbf{L}$ can be split in symmetric part, called the rate of deformation tensor $\mathbf{D}$ and a skew-symmetric part, called the rate of rotation tensor $\boldsymbol{\Omega}$.

$$\mathbf{L} = \mathbf{D} + \boldsymbol{\Omega} \tag{A.13}$$

$$\mathbf{D} = \frac{1}{2}(\mathbf{L} + \mathbf{L}^c) \tag{A.14}$$

$$\boldsymbol{\Omega} = \frac{1}{2}(\mathbf{L} - \mathbf{L}^c) \tag{A.15}$$

A.3 Balance laws

The basic equations of continuum mechanics are the equations of balance, also called the field equations. These laws are descriped in more detail in i.e. Veldpaus [47]. Any isothermal deformation process in a non polar continuum has to satisfy the following three laws, which are given here in a local form:

$$(1)\ \textit{Balance of mass}: \quad \rho J = \rho_0 \tag{A.16}$$

$$(2)\ \textit{Balance of momentum}: \quad \vec{\nabla} \cdot \boldsymbol{\sigma}^c + \rho\vec{q} = \rho\dot{\vec{v}} \tag{A.17}$$

$$(3)\ \textit{Balance of angular momentum}: \quad \boldsymbol{\sigma}^c = \boldsymbol{\sigma} \tag{A.18}$$

where: ρ is the density in the current configuration.
ρ_0 is the density in the refernece configuration.
J is the volume change factor.
$\vec{\nabla}$ is the gradient operator with respect to the current configuration.
$\boldsymbol{\sigma}$ is the Cauchy stress tensor.
$\vec{q}$ is the specific volume force vector.
$\dot{\vec{v}}$ is the material derivate of the velocity vector.

A.4 Constitutive principles

A constitutive equation describes the relation between the stresses and the strains in a material. It is specific for the used material. A number of constitutive principles, derived from physics, can be employed to restrict the possible appearance of the constitutive relations. The most important are summarized below.

The principle of determinism states that the dependent variables in a point P of the continuum with material coordinates $\underset{\sim}{\xi}$ at time t are a function of the independent variables in all points of the body, during the total deformation and temperature history. *The principle of local action* states that the dependent variables in a point P of the continuum with material coordinates $\underset{\sim}{\xi}$ are only a function of the independent variables in the direct neighbourhood of this point during the total deformation and temperature history. The above two principles are incorporated in the definition of a 'simple material'. A 'simple material' is defined as one for which the stress depends only on the history of the deformation tensor $\mathbf{F}$ [29]. From this definition, it follows that:

$$\boldsymbol{\sigma}(\underset{\sim}{\xi}, t) = \overset{t}{\underset{\tau=-\infty}{\mathcal{F}}} \{\mathbf{F}(\underset{\sim}{\xi}, \tau)\} \tag{A.19}$$

where $\mathcal{F}$ is a tensor functional.

A restriction on the manner in which the stress can depend on the deformation tensor arises through *the principle of objectivity* or *frame indifference.* This principle states that the mechanical properties of a material depend only on the material itself and not on the observer. When the consequence of this restriction are applied to the constitutive equation A.19 it can be shown that [29]:

$$\boldsymbol{\sigma}(t) = \mathbf{R}(t) \cdot \overset{t}{\underset{\tau=-\infty}{\mathcal{G}}} \{\mathbf{U}(\tau)\} \cdot \mathbf{R}^c(t) \tag{A.20}$$

where $\mathcal{G}$ is a new arbitrary functional. The relation above shows that the principle of objectivity implies that the current stress depend only on the current value of the orthogonal rotation $\mathbf{R}$ but depends on the entire past history of the stretch $\mathbf{U}$.

The Clausius-Duhem inequality is a special form of the second law of thermodynamics. It states that the internal entropy production must be greater or equal than zero [11]. In this thesis it is not of relevant importance because the deformation is described isothermical.

Appendix B

The Mullins effect

[1]

In this appendix the Mullins effect is explained.

When new samples of (filled) rubber vulcanizates are stretched to a point P and then allowed to retract, subsequent extensions to the same strain require a lower force. In other words the stiffness at all points up to the prestressing limit P is reduced. This effect is normally referred to as stress softening or the 'Mullins effect' after its first investigator [15]. Most of this softening occurs during the first deformation and after some stretching cycles a steady state is reached.

Harwood, Mullins and Payne [20] have shown, by comparing stress softening in both gum and filler loaded vulcanizate, that the softening process is mainly due to the rubber phase alone. Differences between the stress-strain hysteresis loops of gum and filler loaded vulcanizates are caused by an increase in the effective strain in the rubber phase resulting from the presence of a filler. Possible sources for the mechanism of stress softening in gum vulcanizates are [20]:

1. Breaking and remaking of crosslinks during extension.
2. Residual load orientation of network chains persisting after recovery.
3. Breaking of network chains.

The Mullins effect has been mainly investigated with the use of standard tensile extension and recovery tests. The change in the form of the stress-strain curves with respect to a number of cycles to a constant maximum stress or strain is denoted. A typical plot for a tensile specimen subjected to a number of cycles to constant deformation is shown in figure B.1. Roland [39] derived an empirical one dimensional model of the Mullins effect.

In reference [6] hystereses curves are calculated for different rate type models. From these curves it can be concluded that the generalized upperconvected Maxwell equation is capable of describing the Mullins effect.

[1]Reproduced in part from J.J.M. de Bever, Literature survey to the dynamic behaviour of rubber materials, 1992.

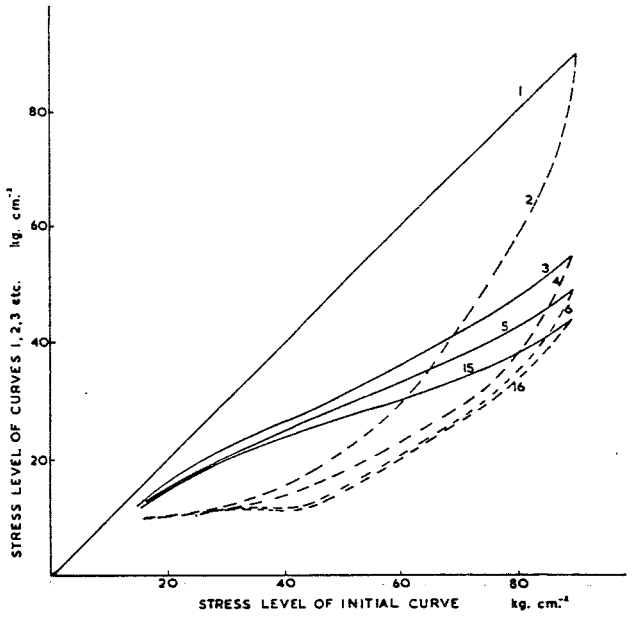

Figure B.1: Comparison of stress levels for repeated cycling of a gum natural rubber vulcanisite (Harwood, Mullins and Payne, 1965)

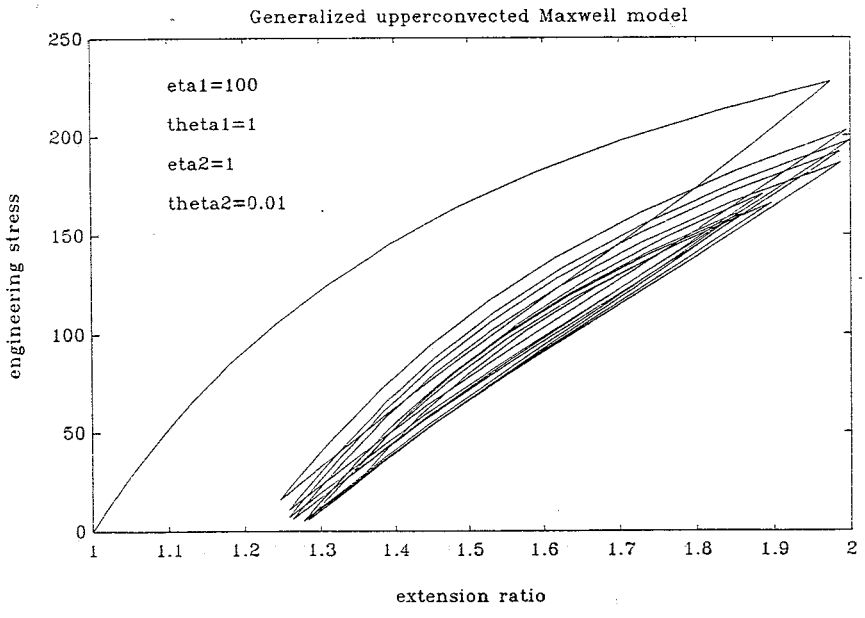

Figure B.2: Hysteresis loops in uniaxial extension, calculated with the use of the generalized upperconvected Maxwell model

Appendix C

Sinusoidal small-amplitude vibrations superposed on finite deformation in viscoelastic solids

In this appendix a constitutive equation is derived which describes the material behaviour of incompressible isotropic viscoelastic materials subjected to small-amplitude time harmonic oscillations superposed on a static finite deformation field.

Coleman and Noll derived a constitutive relation for a compressible isotropic material with fading memory in which only linear terms in the strain history are retained. This theory, which they called finite linear viscoelasticity, can be expressed in the form:

$$\begin{aligned} \boldsymbol{\sigma}(t) \;=\; & -p\mathbf{I} + (\Phi + I_1\Psi)\mathbf{B} - \Psi\mathbf{B}^2 + \\ & \textstyle\sum_{\alpha=0}^{2} \int_{-\infty}^{t} \Phi_\alpha(t-\tau)[\mathbf{B}^\alpha \dot{\mathbf{C}}_t(\tau) + \dot{\mathbf{C}}_t(\tau)\mathbf{B}^\alpha]\, d\tau + \\ & \textstyle\sum_{\alpha=0}^{2}\sum_{\beta=0}^{2} \int_{-\infty}^{t} \Psi_{\alpha\beta}(t-\tau)\mathbf{B}^\alpha \mathrm{tr}[\mathbf{B}^\beta \dot{\mathbf{C}}_t(\tau)]\, d\tau \end{aligned} \qquad \text{(C.1)}$$

where $\boldsymbol{\sigma}$ is the Cauchy stress tensor, $\mathbf{B}$ is the left Cauchy Green strain measure and $\mathbf{C}$ is the right Cauchy Green tensor. Both $\mathbf{B}$ and $\mathbf{C}$ are defined in appendix A. Furthermore p, Φ and Ψ are functions of the current values of the strain invariants I_1, I_2, and I_3, and the twelve relaxation functions Φ_α and $\Phi_{\alpha\beta}$ are functions of time and of I_1, I_2, and I_3. For an incompressible material p becomes an undefined hydrostatic pressure and the terms involving Φ_{00}, Φ_{01}, and Φ_{02} can be absorbed into this term. In addition, since $I_3 = 1$, the material parameters do not depend on this invariant [29].

The class of deformations is considered in which an isotropic incompressible viscoelastic solid, from an undeformed reference configuration Ω_r, is brought to a configuration Ω^0 by applying a finite deformation which is maintained constant for a long time. It is assumed, by invocation of the fading memory principle, that the material is such that when it is held at constant deformation, the resulting stresses

eventually relax to equilibrium values that depend only on the maintained deformation and *not* on the history of deformations imposed previously. This equilibrium state will hereafter be referred to as the delayed elastic response of the material. From equation (C.1) it follows that the constitutive equation for the delayed elastic response may be written in the form:

$$\boldsymbol{\sigma}^0 = -p^0\,\mathbf{I} + 2(W_1 + I_1^0 W_2)\mathbf{B}^0 - 2W_2(\mathbf{B}^0 \cdot \mathbf{B}^0) \tag{C.2}$$

where the superscript 0 denotes the equilibrium state, $W(I_1^0, I_2^0)$ is the equilibrium value of the Helmholtz free energy density, measured per unit volume of the undeformed body, and $W_a = \frac{\partial W}{\partial I_a}$ $(a = 1, 2)$. Comparisson with equation C.1 shows that $\Psi = 2W_2$, and $\Phi = 2W_1$. To this deformation a small dynamic displacement is superposed, which is defined by:

$$\vec{x}(\underset{\sim}{\xi}, t) = \vec{x}^0(\underset{\sim}{\xi}) + \epsilon\Delta\vec{u}(\underset{\sim}{\xi}, t) \tag{C.3}$$

where $\vec{x}^0$ denotes the large static deformation and, $\epsilon\Delta\vec{u}$ denotes the superposed dynamic displacements. ϵ is assumed to be small, so that terms in ϵ^2 are negligible. Lianis [27] has shown that the Cauchy stress tensor $\boldsymbol{\sigma}$ due to the initial deformation and the superposed displacement, within $O(\epsilon^2)$ is given by:

$$\begin{aligned} \boldsymbol{\sigma} \;=\; & -\Delta p\mathbf{I} + \boldsymbol{\sigma}^0 - \boldsymbol{\sigma}^0 \cdot \boldsymbol{\omega} + \boldsymbol{\omega} \cdot \boldsymbol{\sigma}^0 + {}^4\boldsymbol{\Omega}(\mathbf{B}^0) : \mathbf{e} + \\ & 2\int_0^t {}^4\bar{\boldsymbol{\Phi}}((t-\tau);\mathbf{B}^0) : \dot{\mathbf{e}}(\tau)\, d\tau \end{aligned} \tag{C.4}$$

In the above equation Δp is an arbitrary scalar arising as a reaction to the superposed incompressible material motion and $\mathbf{e}$ and $\boldsymbol{\omega}$ are, respectively, the infinitesimal strain and rotation tensors, defined by:

$$\mathbf{e} = \frac{\epsilon}{2}\{(\vec{\nabla}_0\Delta\vec{u}) + (\vec{\nabla}_0\Delta\vec{u})^c\} \tag{C.5}$$

$$\boldsymbol{\omega} = \frac{\epsilon}{2}\{(\vec{\nabla}_0\Delta\vec{u}) - (\vec{\nabla}_0\Delta\vec{u})^c\} \tag{C.6}$$

Where $\vec{\nabla}_0$ is the gradient operator in reference to the initial deformation. Also ${}^4\boldsymbol{\Omega}$ and ${}^4\bar{\boldsymbol{\Phi}}$ are, respectively, the elasticity and stress relaxation tensor defined by [31]:

$${}^4\boldsymbol{\Omega}(\mathbf{B}^0) = \boldsymbol{\sigma} \cdot {}^4\mathbf{I} + {}^4\mathbf{I}^{\mathrm{rc}} \cdot \boldsymbol{\sigma} + p^0({}^4\mathbf{I} + 4\mathbf{I}^{\mathrm{rc}}) + 4\,\mathbf{B}^0 \cdot \frac{\partial^2 W}{\partial\mathbf{C}\,\partial\mathbf{C}} \cdot \mathbf{B}^0 \tag{C.7}$$

$$\begin{aligned} {}^4\bar{\boldsymbol{\Phi}}((t-\tau);\mathbf{B}^0) \;=\; & \Phi_0({}^4\mathbf{I} + {}^4\mathbf{I}^{\mathrm{rc}}) + \Phi_1(\mathbf{B}^0 \cdot {}^4\mathbf{I} + {}^4\mathbf{I}^{\mathrm{rc}}) + \\ & \Phi_2(\mathbf{B}^0 \cdot \mathbf{B}^0 \cdot {}^4\mathbf{I} + {}^4\mathbf{I}^{\mathrm{rc}} \cdot \mathbf{B}^0 \cdot \mathbf{B}^0) + \\ & \Phi_{10}\mathbf{B}^0\mathbf{I} + \Phi_{11}\mathbf{B}^0\mathbf{B}^0 + \Phi_{12}\mathbf{B}^0\mathbf{B}^0 \cdot \mathbf{B}^0 \\ & \Phi_{20}\mathbf{B}^0 \cdot \mathbf{B}^0\mathbf{I} + \Phi_{21}\mathbf{B}^0 \cdot \mathbf{B}^0\mathbf{B}^0 + \Phi_{22}\mathbf{B}^0 \cdot \mathbf{B}^0\mathbf{B}^0 \cdot \mathbf{B}^0 \end{aligned} \tag{C.8}$$

It should be noted that the fourth order tensors ${}^4\mathbf{I}$ and ${}^4\mathbf{I}^{\mathrm{rc}}$ are defined such that [7]:

$$ {}^4\mathbf{I} : \mathbf{A} = \mathbf{A} \tag{C.9} $$

and

$$ {}^4\mathbf{I}^{\mathrm{rc}} : \mathbf{A} = \mathbf{A}^{\mathrm{c}} \tag{C.10} $$

The superposed small deformation is chosen to be a time harmonic sinusoidal vibration of frequency ω. Thus:

$$ \Delta\vec{u} = \Delta\vec{u}^*(\omega)\exp(i\omega t) \tag{C.11} $$

and consequently:

$$ \Delta p = \Delta p^*(\omega)\exp(i\omega t) \tag{C.12} $$

$$ \mathbf{e} = \mathbf{e}^*(\omega)\exp(i\omega t) \tag{C.13} $$

$$ \boldsymbol{\omega} = \boldsymbol{\omega}^*(\omega)\exp(i\omega t) \tag{C.14} $$

The superscript * denotes a complex valued function of frequency ω. Substitution of the above four equations in equation C.4 results after performing the intergration in:

$$ \boldsymbol{\sigma} = \boldsymbol{\sigma}^0 + \Delta\boldsymbol{\sigma}^*\exp(i\omega t) \tag{C.15} $$

with:

$$ \Delta\boldsymbol{\sigma}^* = -\Delta p^*\,\mathbf{I} + \boldsymbol{\omega}^*\cdot\boldsymbol{\sigma}^0 - \boldsymbol{\sigma}^0\cdot\boldsymbol{\omega}^* + [{}^4\boldsymbol{\Omega}(\mathbf{B}^0) + 2i\omega\,{}^4\boldsymbol{\Phi}(\omega;\mathbf{B}^0)] : \mathbf{e}^* \tag{C.16} $$

Furthermore the material is assumed to be incompressible, which means that:

$$ \mathrm{tr}\,\mathbf{e} = 0 \tag{C.17} $$

For further purposes equation C.15 will be rewritten in terms of the second Piola Kirchhoff stress tensor and the Lagrangian strain. The second Piola Kirchhoff stress tensor is defined by:

$$ \mathbf{S} = J\mathbf{F}^{-1}\cdot\boldsymbol{\sigma}\cdot\mathbf{F}^{-c} \tag{C.18} $$

Where $\mathbf{F}$ is the deformation tensor and J is the volume change ratio. The latter equals 1 for an incompressible material. The Lagrangian strain is defined as:

$$ \mathbf{E} = \frac{1}{2}(\mathbf{C} - \mathbf{I}) \tag{C.19} $$

The incremental part of the Green-Lagrange strain tensor $\Delta\mathbf{E}$ can be split in a linear part $\Delta\boldsymbol{\epsilon} = (\mathbf{F}^0)^c \cdot \mathbf{e} \cdot \mathbf{F}$ and a nonlinear part $\Delta\boldsymbol{\eta}$. Application of equations C.18 and C.19 in equation C.15 yields within $O(\epsilon^2)$:

$$\mathbf{S} = \mathbf{S}^0 + \Delta\mathbf{S}^* \exp(i\omega t) \tag{C.20}$$

$$\mathbf{S}^0 = -p^0(\mathbf{C}^0)^{-1} + 2(W_1 + I_1^0 W_2)\mathbf{I} - 2W_2\mathbf{C}^0 \tag{C.21}$$

$$\Delta\mathbf{S}^* = -\Delta p^*(\mathbf{C}^0)^{-1} + {}^4\mathbf{L}^* : \Delta\boldsymbol{\epsilon}^* \tag{C.22}$$

with:

$${}^4\mathbf{L} = {}^4\mathbf{D} + 2i\omega\, {}^4\boldsymbol{\Phi}^*(\omega; \mathbf{C}^0) \tag{C.23}$$

In the above equation ${}^4\mathbf{D}$ and ${}^4\boldsymbol{\Phi}$ are, respectively the elasticity tensor and the complex valued relaxation tensor, defined by:

$${}^4\mathbf{D} = p_0\{\mathbf{C}^{-1} \cdot {}^4\mathbf{I} \cdot \mathbf{C}^{-1} + \mathbf{C}^{-1} \cdot {}^4\mathbf{I}^{rc} \cdot \mathbf{C}^{-1}\} + 4\,\frac{\partial^2 W}{\partial\mathbf{C}\,\partial\mathbf{C}} \tag{C.24}$$

$$\begin{aligned} {}^4\boldsymbol{\Phi}^* \;=\; & \Phi_0^*[\mathbf{C}^{-1} \cdot {}^4\mathbf{I} \cdot \mathbf{C}^{-1} + \mathbf{C}^{-1} \cdot {}^4\mathbf{I}^{rc} \cdot \mathbf{C}^{-1}] + \\ & \Phi_1^*[{}^4\mathbf{I}^{rc} \cdot \mathbf{C}^{-1} + \mathbf{C}^{-1} \cdot {}^4\mathbf{I}] + \\ & \Phi_2^*[\mathbf{C} \cdot {}^4\mathbf{I} \cdot \mathbf{C}^{-1} + \mathbf{C}^{-1} \cdot {}^4\mathbf{I}^{rc} \cdot \mathbf{C}] + \\ & \Phi_{10}^*\mathbf{I}\mathbf{C}^{-1} + \Phi_{11}^*\mathbf{I}\mathbf{I} + \Phi_{12}^*\mathbf{I}\mathbf{C} + \\ & \Phi_{20}^*\mathbf{C}\mathbf{C}^{-1} + \Phi_{21}^*\mathbf{C}\mathbf{I} + \Phi_{22}^*\mathbf{C}\mathbf{C} \end{aligned} \tag{C.25}$$

Appendix D

Relaxation functions

Morman [31] presented simplifications, based on the assumption that the material exhibits seperability of time and strain. These simplifications lead to explicit expressions for the nine complex valued scalar relaxation functions. In this appendix the relaxation functions as proposed by Morman are presented and are expressed in terms of the material constants η_i and θ_i.

The relaxation functions are given by:

$$\Phi_0^*(\omega) = 2g^*(\omega)I_2W_2 \tag{D.1}$$

$$\Phi_1^*(\omega) = 2g^*(\omega)(W_1 - I_1W_2) \tag{D.2}$$

$$\Phi_2^*(\omega) = 2g^*(\omega)W_2 \tag{D.3}$$

$$\Phi_{10}^*(\omega) = 4g^*(\omega)I_1W_2 \tag{D.4}$$

$$\Phi_{11}^*(\omega) = 4g^*(\omega)(W_{11} + 2I_1W_{12} + I_1^2W_{22}) \tag{D.5}$$

$$\Phi_{12}^*(\omega) = \Phi_{21}^*(\omega) = -4g^*(\omega)(W_{12} + I_1W_{22}) \tag{D.6}$$

$$\Phi_{20}^*(\omega) = -4g^*(\omega)W_2 \tag{D.7}$$

$$\Phi_{22}^*(\omega) = 4g^*(\omega)W_{22} \tag{D.8}$$

Due to the incompressibility constraint given by $\mathrm{tr}\,\epsilon = 0$ it can easily be shown that $\mathbf{C}^{-1} : \epsilon = 0$. Thus the terms containing Φ_{10}^* and Φ_{20}^* may be omitted from equation (C.25).

In the above set of equations $g^*(\omega)$ is given by:

$$g^*(\omega) = \int_0^\infty g(t)\exp(-i\omega t)\,dt \tag{D.9}$$

and:

$$g(t) = \frac{1}{2}\left(\frac{G(t)}{G_e} - 1\right) \tag{D.10}$$

where $G(t)$ is the shear relaxation modulus of linear viscoelsticity and G_e is the long time equilibrium shear modulus.

The expression for the relaxation modulus that corresponds to multi-mode Maxwell behaviour is given by [14]:

$$G(t) = G_e + \sum_{i=1}^{N} \frac{\eta_i}{\theta_i} \exp(\frac{-t}{\theta_i}) \tag{D.11}$$

Thus:

$$g^*(\omega) = \int_0^\infty \frac{1}{2}\frac{1}{G_e} \sum_{i=1}^{N} \frac{\eta_i}{\theta_i} \exp(-t(\frac{1}{\theta_i} + i\omega)\, dt \tag{D.12}$$

Performing the intergration results in:

$$g^*(\omega) = \frac{1}{2}\frac{1}{G_e} \sum_{i=1}^{N} \frac{\eta_i}{\theta_i} \frac{1}{\frac{1}{\theta_i} + i\omega} \quad \text{with } \mathrm{Re}(\frac{1}{\theta_i} + i\omega) > 0 \tag{D.13}$$

Appendix E

The material behaviour of elastomers in MARC

MARC is a general purpose nonlinear finite element code. For the three-dimensional analysis of elastomers, the code uses second-order isoparametric elements in a mixed variational formulation: the displacements are interpolated through quadratic functions, whereas the pressure variables are interpolated from the corner nodes only. Both displacements and pressures are assumed to be continuous [31].

The isothermal mechanical analysis of incompressible rubber materials in which a small amplitude time harmonic oscillation is superposed on a static finite deformation field consits in MARC of the following steps:

1. Calculation of the nonlinear response of the rubber material to a static preload based on the constitutive equation (C.21) for the delayed elastic material response. In this portion of the analysis viscous and inertia effects are neglected.

2. The complex valued amplitudes of the superimposed response are calculated at each given frequency and amplitude for the boundary tractions and/or displacements. Both viscoelastic material behaviour and inertia effects are considered.

In MARC the third order invariant form of the potential function $W(I_1, I_2)$ by James, Green and Simpson has been implemented:

$$\begin{aligned} W(I_1, I_2) &= C_{10}(I_1 - 3) + C_{01}(I_2 - 3) + C_{11}(I_1 - 3)(I_2 - 3) \\ &\quad + C_{20}(I_1 - 3)^2 + C_{30}(I_1 - 3)^3 \end{aligned} \tag{E.1}$$

Mooney-Rivlin material behaviour is obtained by choosing C_{11}, C_{20} and C_{30} equal to zero. By also setting C_{01} to zero Neo-Hookean material behaviour is obtained. The constants can be obtained from experimental data by least square fit on the isochronal stress-strain curve The potential function is available through the Mooney option.

The relaxation functions are defined through the PHI-function option. A user-subroutine can be written to define these relaxation functions. In appendix D the relaxation functions are expressed in terms of the material constants η_i and θ_i, which can be obtained from linear viscoelastic measurements.

The superposed sinusoidal displacements are available through the Harmonic option [30].

Appendix F

The Maxwell model in stress relaxation

In this appendix the behaviour of the upperconvected Maxwell model and the multimode Maxwell model in uniaxial stress relaxation is calculated. The upperconvected Maxwell model is given by:

$$\left.\begin{array}{rcl} \boldsymbol{\sigma} & = & -p\mathbf{I}+\boldsymbol{\tau} \\ \overset{\nabla}{\boldsymbol{\tau}}+\frac{1}{\theta}\boldsymbol{\tau} & = & \frac{2\eta}{\theta}\mathbf{D} \end{array}\right\} \tag{F.1}$$

where $\boldsymbol{\sigma}$ is the Cauchy stress, p is an isotropic constant, $\mathbf{I}$ is the unity tensor, θ is a time constant, η is a viscocity, $\boldsymbol{\tau}$ is the extra stress tensor, $\mathbf{D}$ is the rate of deformation tensor, and $\overset{\nabla}{\boldsymbol{\tau}}$ is the Truesdell rate of the extra stress tensor, defined by:

$$\overset{\nabla}{\boldsymbol{\tau}}=\dot{\boldsymbol{\tau}}-\mathbf{L}\cdot\boldsymbol{\tau}-\boldsymbol{\tau}\cdot\mathbf{L}^{c} \tag{F.2}$$

where $\mathbf{L}$ is the velocity gradient tensor. $\mathbf{L}=\mathbf{O}$ in a stress relaxation experiment. Thus in a stress relaxation experiment the upperconvected Maxwell model reduces to:

$$\left.\begin{array}{rcl} \boldsymbol{\sigma} & = & -p\mathbf{I}+\boldsymbol{\tau} \\ \dot{\boldsymbol{\tau}}+\frac{1}{\theta}\boldsymbol{\tau} & = & \mathbf{O} \end{array}\right\} \tag{F.3}$$

The solution of the above homogenous differential equation is given by:

$$\boldsymbol{\tau}=\mathbf{C}\exp\frac{-t}{\theta} \tag{F.4}$$

The stress relaxation experiments are conducted in uniaxial extension. Therefore only one stress component (σ_{11}) is unequal to zero . It then can be easily deduced that $\tau_{22}=\tau_{33}=p$. The tensile stress is given by:

$$\sigma_{11}=C_{11}\exp\frac{-t}{\theta}-C_{22}\exp\frac{-t}{\theta}=c\exp\frac{-t}{\theta} \tag{F.5}$$

The second model used to fit the data is the generalized Maxwell model. This model can be considered as a summation of n upperconvected Maxwell models. The stress relaxation function is given by:

$$\sigma_{11} = \sum_{i=1}^{n} c_i \exp \frac{-t}{\theta_i} \tag{F.6}$$

Appendix G

The rheometrics RDS-2

The rheometrics RDS-2 is a rotational rheometer with which the relaxation behaviour in shear and the dynamic moduli can be obtained. A sample of the material is held between two discs, steady rotation of one of the discs causes a shear strain in the material, and at the other disc the resulting force is measured. This type of measurement configuration is usually referred to as gap loading. The discs can have different shapes. The most common shapes are cone and plate and parallel plate discs, see figure G.1. The rheometrix RDS-2 uses both the above shapes.

For the parallel plate geometry the shear velocity $\dot{\gamma}$ is given by [22]:

$$\dot{\gamma} = \frac{R\omega}{H} \tag{G.1}$$

where: R is radius.
ω is angular frequency.

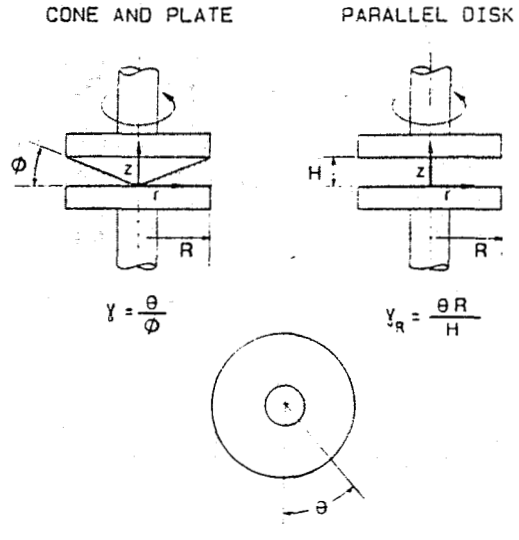

Figure G.1: Sketch of cone-and-plate and parallel-disc geometries (Soskey and Winter, 1984).

H is the distance between the discs.

For the cone-and-plate geometry it follows that:

$$\dot{\gamma} = \frac{\omega}{\tan \Phi} \tag{G.2}$$

and for small Φ this reduces to:

$$\dot{\gamma} = \frac{\omega}{\Phi} \tag{G.3}$$

where Φ is the angle between cone and plate. The shear velocity for the cone and plate geometry is everywhere in the material the same, contrary to the parallel plate disc geometry where the shear velocity is a function of the radius. This difference becomes important when the total history of shear appears in the viscosity function. The plate-and-cone geometry then has the preference because the history of each material particle is the same. However it has the disadvantage that the sample preparation is more difficult.

Appendix H

The WLF equation

In this appendix the Williams, Landel, Ferry (WLF) equation is derived from free volume theory and the principle of time temperature superposition is explained.

A polymeric liquid or soft solid is considered to consist of a volume occupied by the liquid molecules V_o, plus some free volume V_f. V_o includes not only the volume of the molecules as represented by their van der Waals radii, but also the volume associated with vibrational motion. V_f may be present as holes of the order of molecular dimensions or smaller voids associated with packing irregularities, into which the molecules move as they undergo Brownian motion. The fractional free volume f is defined as the free volume divided by the total volume, and since in most instances $V_f << V_o$:

$$f \approx \frac{V_f}{V_o} \tag{H.1}$$

It may be assumed that f increases linear with temperature in accordance with the relation:

$$f = f_g + \alpha(T - T_g) \tag{H.2}$$

where : f_g = fractional free volume at T_g.
α = $\alpha_T - \alpha_g$.
α_T = thermal expansion coefficient above T_g.
α_g = thermal expansion coefficient below T_g.
T_g = glass transition temperature.
T = temperature above T_g.

The glass transition temperature is that temperature at which the thermal expansion coefficient undergoes a discontinuity and below which configurational rearrangements of polymers are extremely slow.

It is believed that the molecular mobility at any temperature depends primarily on the free volume remaining. This concept was applied by Doolittle [19] with the following emperical expression:

$$\ln \eta_T = \ln A + \frac{1}{f} \tag{H.3}$$

where: η_T = viscosity at temperaure T.
A = constant.

If the above equation is written for temperatures T and T_g, and the two resulting equations are then subtracted,

$$\log\left(\frac{\eta_T}{\eta_g}\right) = \frac{1}{2.303}\left(\frac{1}{f} - \frac{1}{f_g}\right) \tag{H.4}$$

where η_g is the viscosity at T_g. Combining equations H.2 and H.4 yields:

$$\log\left(\frac{\eta_T}{\eta_g}\right) = \frac{-c_1^g(T - T_g)}{c_2^g + (T - T_g)} \tag{H.5}$$

where:

$$c_1^g = \frac{1}{2.303 f_g} \tag{H.6}$$

and

$$c_2^g = \frac{f_g}{\alpha} \tag{H.7}$$

This equation has come to be known as the WLF-equation. In the first application of it average values of c_1^g and c_2^g were obtained on a large number of polymers and estimated to be 17.44 and 51.6 respectively. With the use of these specific values, the above equation is called the universal WLF-equation. It is evident that the actual variation from one polymer to another is too great to permit use of these 'universal' constant unless as a last resort when no other data is available [14].

It is also possible to write the WLF-equation for an arbitrary reference temperature (above T_g), T_0:

$$\log\left(\frac{\eta_T}{\eta_{T_0}}\right) = \frac{-c_1(T - T_0)}{c_2 + (T - T_0)} \tag{H.8}$$

with:

$$c_1 = \frac{c_1^g c_2^g}{c_2^g + T_0 - T_g} \tag{H.9}$$

and

$$c_2 = c_2^g + T_0 - T_g \tag{H.10}$$

An alternative interpretation of the ratio $\frac{\eta_T}{\eta_{T_0}}$ can be given. Due to enhanced molecular mobility, the viscosity of a polymer decreases as the free volume increases. This mobility can be seen as involving successive jumps of molecular segments into holes. The larger the number of holes, the larger the jump frequency Φ. Thus a higher jump frequency would result in a lower viscosity. If it is assumed that the jump frequency and the viscosity are inversely related, it follows that:

$$\frac{\eta_T}{\eta_{T_0}} = \frac{\Phi_{T_0}}{\Phi_T} \tag{H.11}$$

It is customary to define:

$$a_{T_0} = \frac{\Phi_{T_0}}{\Phi_T} \tag{H.12}$$

where a_{T_0} is called the horizontal shift factor.

The utility of the WLF-equation can be demonstrated as follows. Consider for instance, the dynamic modulus G^* of an amorphous polymer. At any given temperature G^* increases with increasing test frequency. This stiffening is due to the smaller number of jumps (relaxational motions) which can take place during the deformation cycle at the higher test frequency. Similarly, as temperature decreases, at any fixed frequency, the molecular jump frequency is reduced, thus G^* increases,due to diminished free volume. This opposite influency of test temperature and test frequency is referred to as time-temperature superposition. In order to assure that $G^*(T, \omega_T)$ $= G^*(T_0, \omega_{T0})$, where ω_T is the test frequency at temperature T, it is required that at the two test conditions, (T, ω_T) and (T_0, ω_{T0}), the number of relaxation motions (jumps) during a test cycle is constant. Then:

$$\frac{\Phi_T}{\omega_T} = \frac{\Phi_{T_0}}{\omega_{T_0}} \tag{H.13}$$

Combination of equations H.12 and H.13 yields:

$$a_T \omega_T = \omega_{T0} \tag{H.14}$$

In this manner using a_T to shift the results, the frequency scale of the measured mechanical property may be extended, resulting in a master curve over a much broader frequency interval [19].

Appendix I

Derivation of the discrete viscoelastic spectra

In this appendix an expression is derived for the dynamic moduli G' and G''.

In the range of small deformations, the relation between the stress and strain can be described by a constitutive equation of the form [4]:

$$\boldsymbol{\tau}(t) = \int_{-\infty}^{t} G(t-t')\,\dot{\boldsymbol{\gamma}}(t')\,dt' \tag{I.1}$$

where $\boldsymbol{\tau}$ is the stress tensor.

$\dot{\boldsymbol{\gamma}}$ is the strain rate tensor.

$G(t)$ is the linear relaxation modulus.

The form of the time dependence of $G(t)$ or the frequency dependence of $G'(\omega)$ and $G''(\omega)$ can be imitated by the behaviour of a mechanical model consisting of springs and dashpots. The expression for the relaxation modulus G(t) that corresponds to multi-mode Maxwell behaviour (N parallel sets of a spring in serie with a dashpot) is given by [14]:

$$G(t) = G_e + \sum_{i=1}^{N} g_i \exp(\frac{-t}{\theta_i}) \tag{I.2}$$

Where each spring i corresponds to a shear rigidity g_i and each dashpot to a viscosity η_i. The relaxation time θ_i is then defined as $\frac{\eta_i}{g_i}$. For a viscoelastic solid, one of the relaxation times must be infinite and the corresponding modulus contribution is G_e.

When the input is a sinusoidally varied deformation with an angular frequency ω of the form:

$$\gamma_{12} = \gamma_0 \cos(\omega t) \tag{I.3}$$

where γ_{12} = the shear strain.

γ_0 = the shear strain amplitude.

t = the time.

and the amplitude is small, then the shear stress τ_{12} will be sinusoidal with frequency ω, but with a different amplitude and not in phase with the strain input.

$$\tau_{12} = \tau_0 \cos((\omega t) + \delta) = \tau_0 \{\cos(\omega t)cos(\delta) - \sin(\omega t)\sin(\delta)\} \tag{I.4}$$

The shear storage modulus G', which is in phase with the strain (elastic respons),is defined by:

$$G'(\omega) = \frac{\tau_0}{\gamma_0} cos\{\delta(\omega)\} \tag{I.5}$$

Further the loss modulus, which is $\frac{\pi}{2}$ radians out of phase with the strain input (viscous respons),is defined by:

$$G'' = \frac{\tau_0}{\gamma_0} \sin\{\delta(\omega)\} \tag{I.6}$$

Substitution of equations I.5 and I.6 in equation I.4 yields:

$$\tau_{12} = \gamma_0\{G'(\omega)\ \cos(\omega t) - G''(\omega)\ \sin(\omega t)\} \tag{I.7}$$

Differentation of equation I.3 yields, after substitution in equation I.1:

$$\tau_{12} = -\omega\gamma_0 \int_{-\infty}^{t} G(t - t')sin(\omega t')\, dt' \tag{I.8}$$

Substitution of equation I.2 in equation I.8 and application of equation I.7 results after intergration in:

$$G'(\omega) = G_e + \sum_{i=1}^{N} g_i \frac{(\omega\theta_i)^2}{1 + (\omega\theta_i)^2} \tag{I.9}$$

$$G''(\omega) = \sum_{i=1}^{N} g_i \frac{(\omega\theta_i)}{1 + (\omega\theta_i)^2} \tag{I.10}$$

Appendix J

Results of preleminary DMTA and DSC eperiments

In this appendix the differences that occur for silicone rubber between the results obtained in shear and the results obtained in a stress relaxation experiment are further investigated. As a first step dynamic mechanical thermal analysis (DMTA) was conducted. The results of these measurements were further investigated with differential scanning calorimetry (DSC).

Dynamic mechanical thermal analysis involves applying an oscillating mechanical strain and resolving the strain into real and imaginary components. This procedure essentially detects all changes in the state of molecular motion as temperature is scanned. In this way it is possible to detect the glass transition temperature. However it should be noted that the exact location found for T_g will depend on the thermal history of the sample, the rate at which the temperature is scanned during the measurement, and the characteristic time scale of the measuring probe. If one measuring technique senses molecular motions at a higher frequency than another, the apparent discontinuity in behaviour appears at higher temperatures for the higher-frequency technique [12].

DMTA-measurements are conducted on a sample of butyl rubber (size 14.6 mm^2 by 32.9 mm) and on a sample of silicone rubber (size 14.6 mm^2 by 29.2 mm). The rate at which the temperature was scanned was $2\,^{\circ}C$ in both cases. Figure J.1 is a typical plot of a DMTA-experiment on a crosslinked rubber material. The tensile modeulus E is at low temperatures approximately 4 GPa, which is characteristic for the glassy region. In this region the rubber is hard and rigid and behaves like a glass. By increasing the temperature a transition occurs; the modulus and viscosity decrease rapidly through several orders of magnitude in a small temperature range. This transition is identified with the so-called 'glass-transition'. For butyl this transition occurs at -31 $^{\circ}C$. Above the glass-transition temperature, the material behaves as a rubber.

In figure J.2 the result of a DMTA-measurement on silicone rubber is shown. It can be seen that a transition, which is identified as the glass-transition, occurs

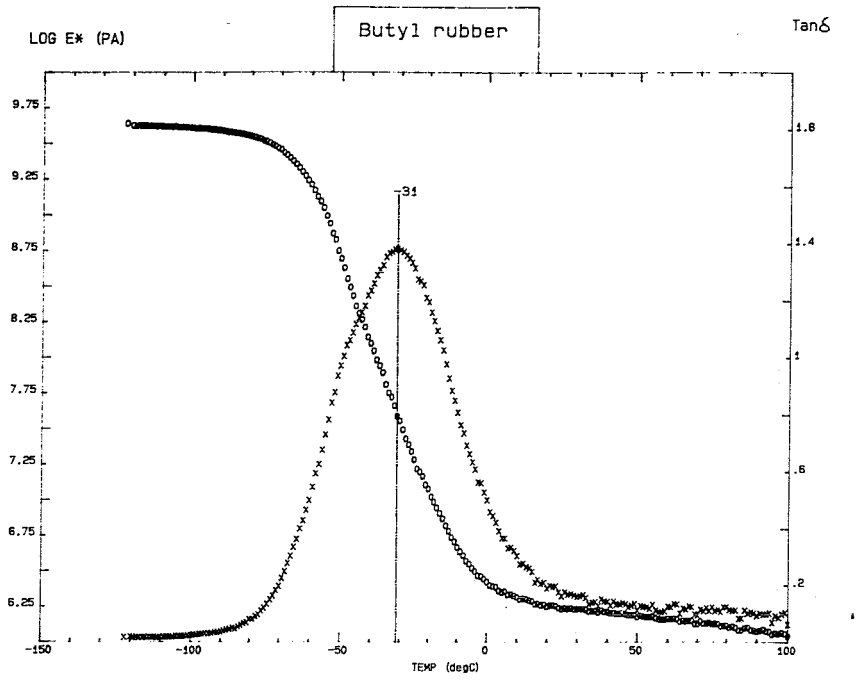

Figure J.1: DMTA of butyl rubber (Dynamic modulus: o, tan δ: x).

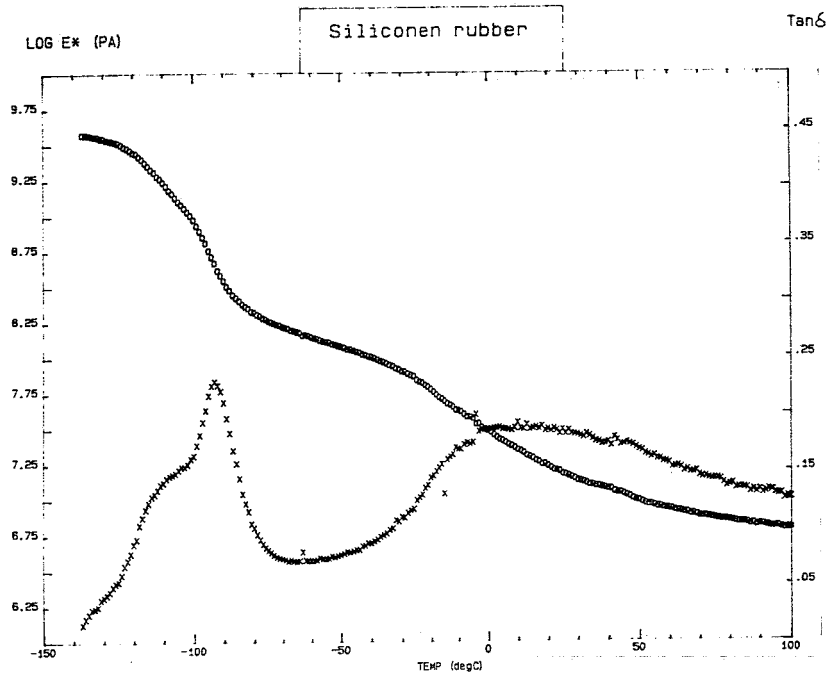

Figure J.2: DMTA of silicone rubber (Dynamic modulus: o, tan δ: x).

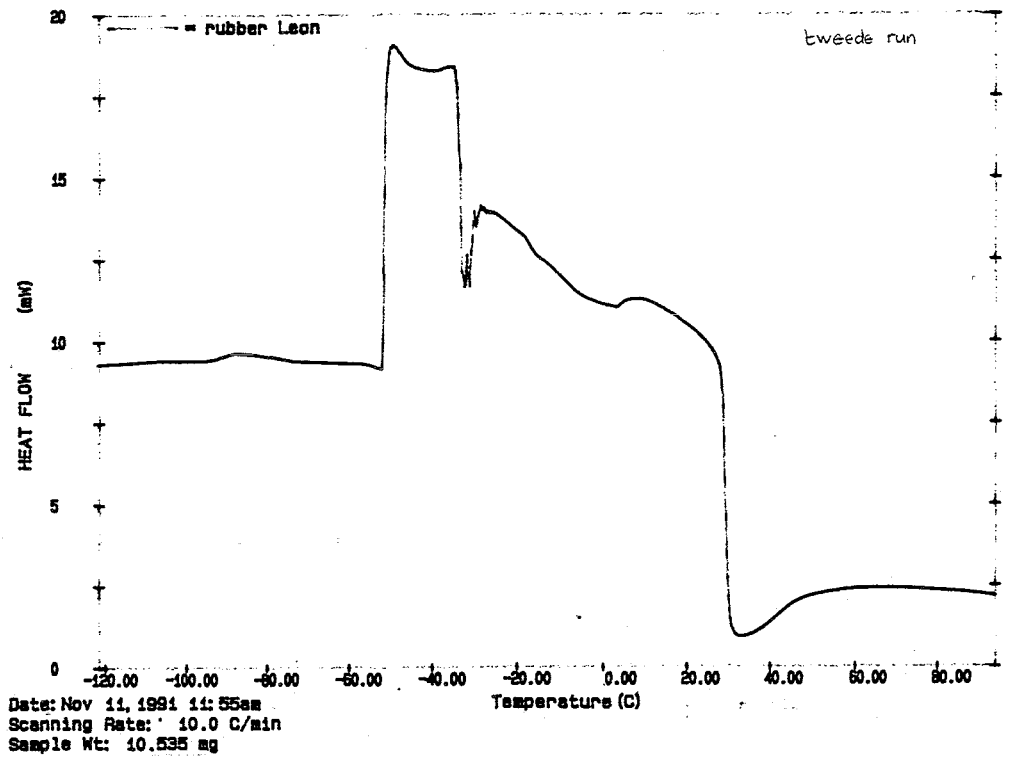

Figure J.3: DSC of silicone rubber

at approximately -100 $^{\circ}C$ However at approximately -50 $^{\circ}C$ a second transition occurs. The tensile modulus E is then approximately 100 MPa, which is a typical value of a crystalline transition. This crystalline transition can be due to either α-relaxation or melting. In the first case annealing causes morphology[1] changes. In the latter case crystals disappear. The crystalline transition is further investigated with DSC-experiments.

For silicone rubber preleminary DSC-measurements were conducted by Tervoort-Engelen. The results of the second run are shown in figure J.3. When the sample undergoes a discrete change in heat capacity, this shows up as a discontinuity in the smooth baseline. The first discontinuity occurs at -90 $^{\circ}C$ and can be identified with the glass transition. At approximatelly the sam temperature as in the DMTA-scan a second discontinuity occurs. However this transition is rather strange and the system does not return to its orginal baseline [12, 18]. Further investigation of this transition is outside the field of this work.

[1]The morphology of a material is its organization on a supra molecular scale, i.e. the form, size and orientation of its crystallites, domains, the structure of groups of molecules in the specimen and of their boundaries and the degree of crystallinity.

Acknowledgements

The author wishes to thank Yvonne Tervoort-Engelen for conducting the DSC-experiments. Moreover the support of Leon Govaert in performing the DMTA-experiments and in interpreting the results of both the DMTA and the DSC measurements is gratefully acknowledged.

Appendix K

Hysteresis curves in uniaxial tension

In this appendix the results of computer simulations of hysteresis curves in uniaxial tension are shown. The calculations are performed with the finite element package SEPRAN, in which the multi-mode Maxwell model has been implemented.

The tension test is simulated on a rectangular bar, by prescribing a displacement in the direction of the 'tensile force'. The boundary conditions are such that the extension is uniaxial. The tests are conducted with different 'strain-rates'. The used strain-rate is defined as follows:

$$\text{strain-rate} = \frac{\Delta L}{L_0 \, \Delta t} \tag{K.1}$$

where ΔL is the prescribed displacement, L_0 is the original length of the bar and Δt is the time step. The results of the computer simulations are shown in figures K.1 to K.4. For butyl rubber the results are compared with a hysteresis test on a butyl rubber ring, conducted with the same strain-rate. No attempt at this time has been made for comparing the results of silicone rubber with experimental data, because in chapter 4 it has been shown that the model predictions of stress-relaxation of silicone rubber are not in accordance with experimental data. This is probably due to the semi-crystallinety of the silicone rubber.

Acknowledgements

The author wishes to thank Frans Paridaans for providing the experimental data of a hysteresis loop of butyl rubber.

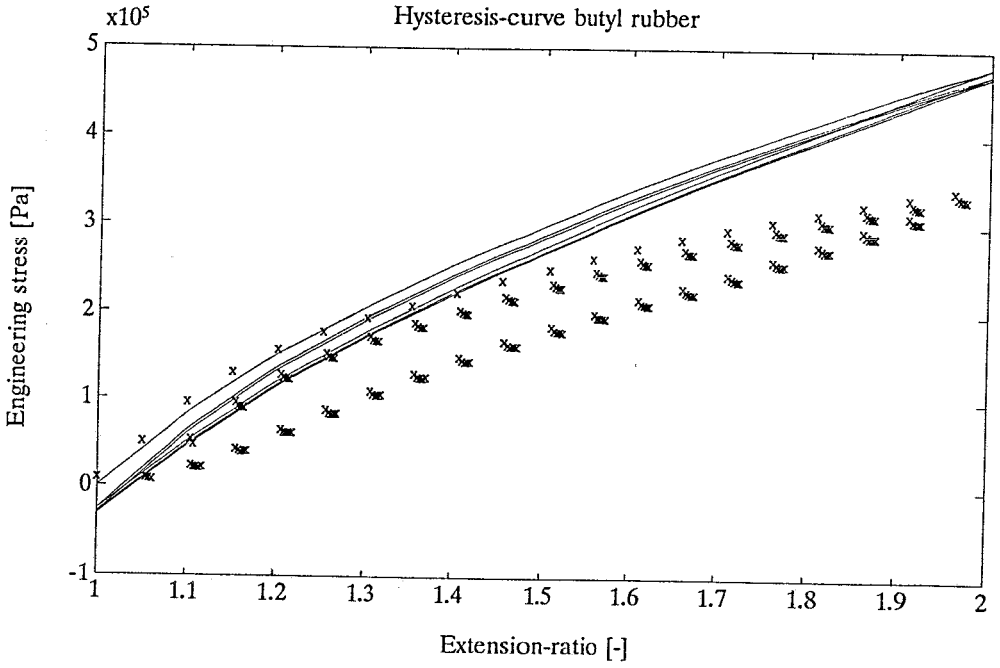

Figure K.1: Hysteresis loop of butyl rubber in uniaxial extension, strain velocity 325 %/min, computer simulation:- ,experimental: x.

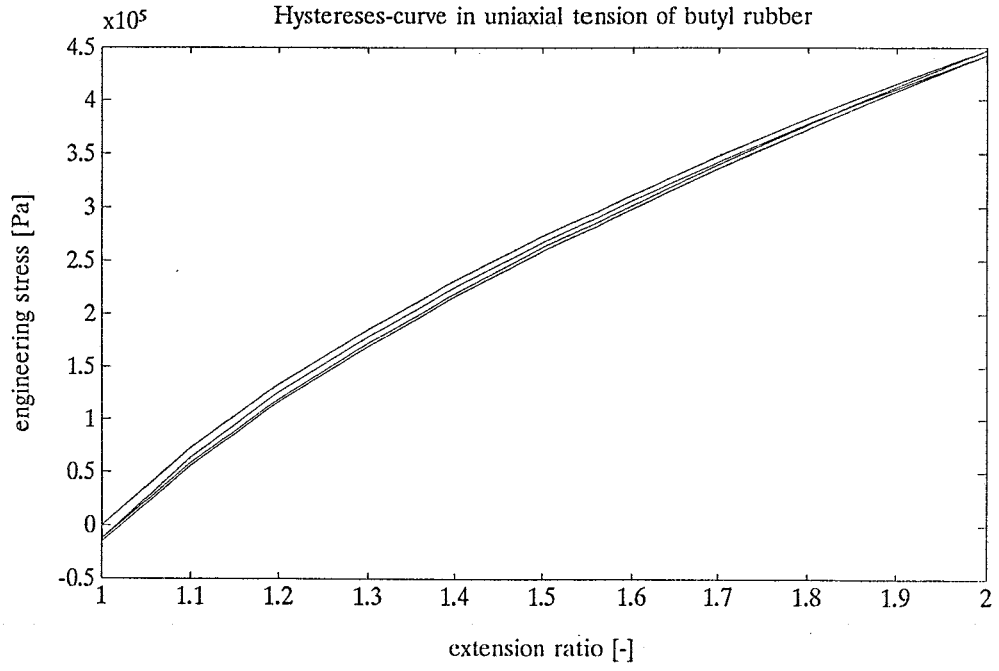

Figure K.2: Hysteresis loop of butyl rubber in uniaxial extension, strain velocity 10 %/min.

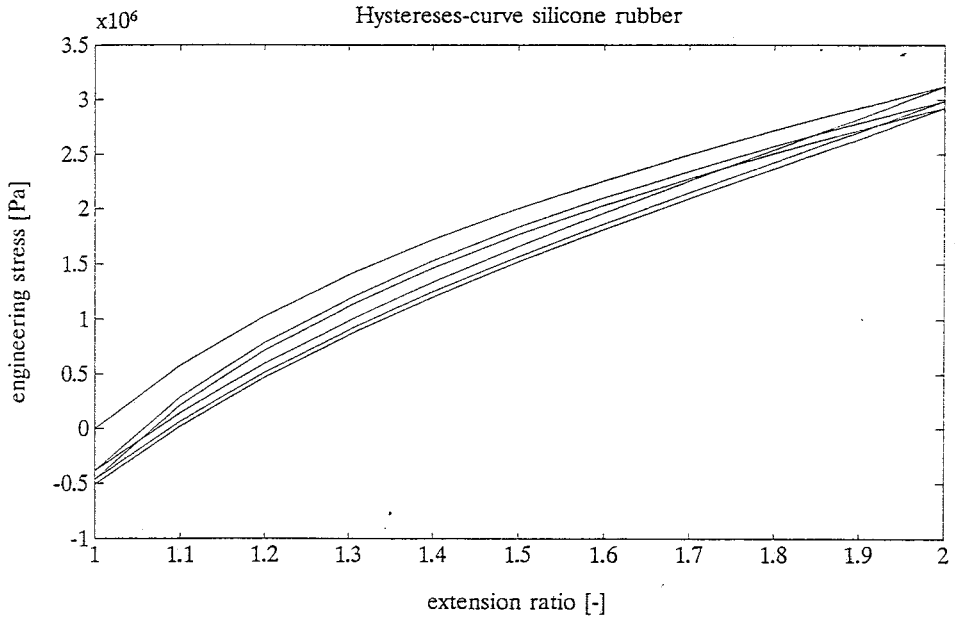

Figure K.3: Hysteresis loop of silicone rubber in uniaxial extension, strain velocity 5000 %/min.

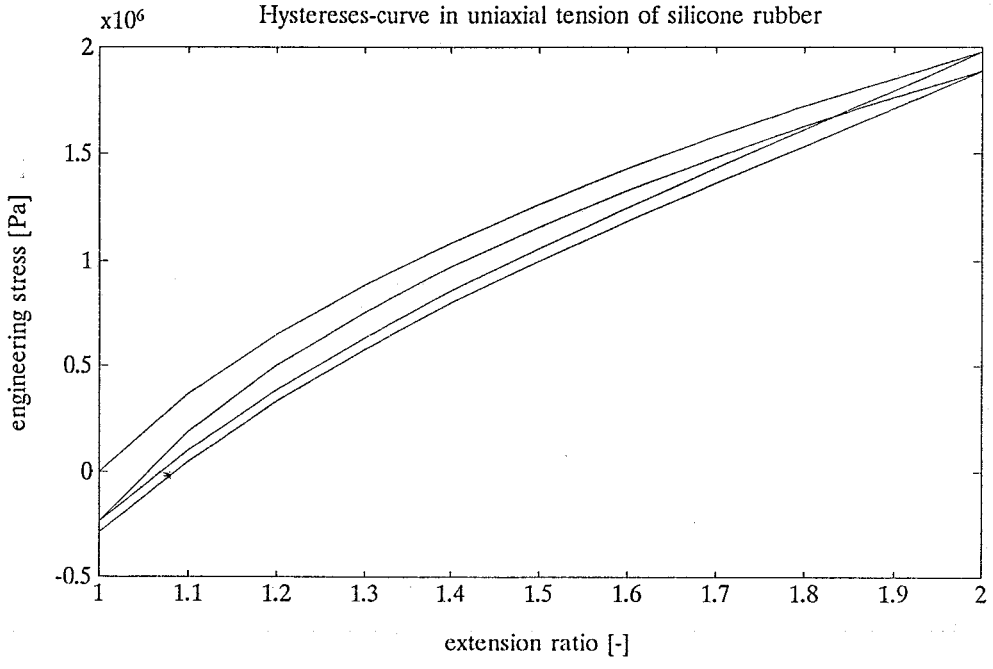

Figure K.4: Hysteresis loop of butyl rubber in uniaxial extension, strain velocity 10 %/min.

Appendix L

Hysteresis curves in uniaxial compression.

In this appendix the results of computer simulations, with the finite element code SEPRAN, of hysteresis curves in uniaxial compression are shown.

Two geometries are used to simulate the hysteresis curve. The first geometry is a cube consisting of 2 x 2 x 2 elements. The second geometry is a hollow pipe. In figure L.1 the undeformed and deformed pipe geometry are shown. The boundary conditions are such that the compression is uniaxial.

The results of the computer simulations are shown in figures L.2 to L.7.

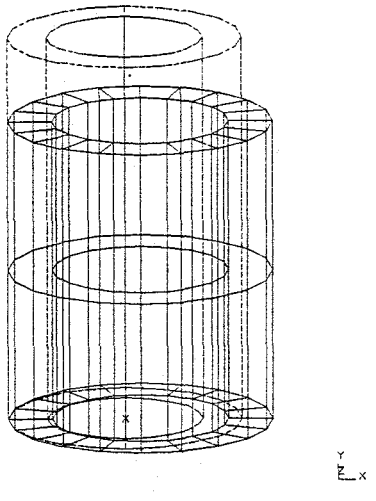

Figure L.1: Pipe geomety, undeformed: dashed line, deformed: solid line.

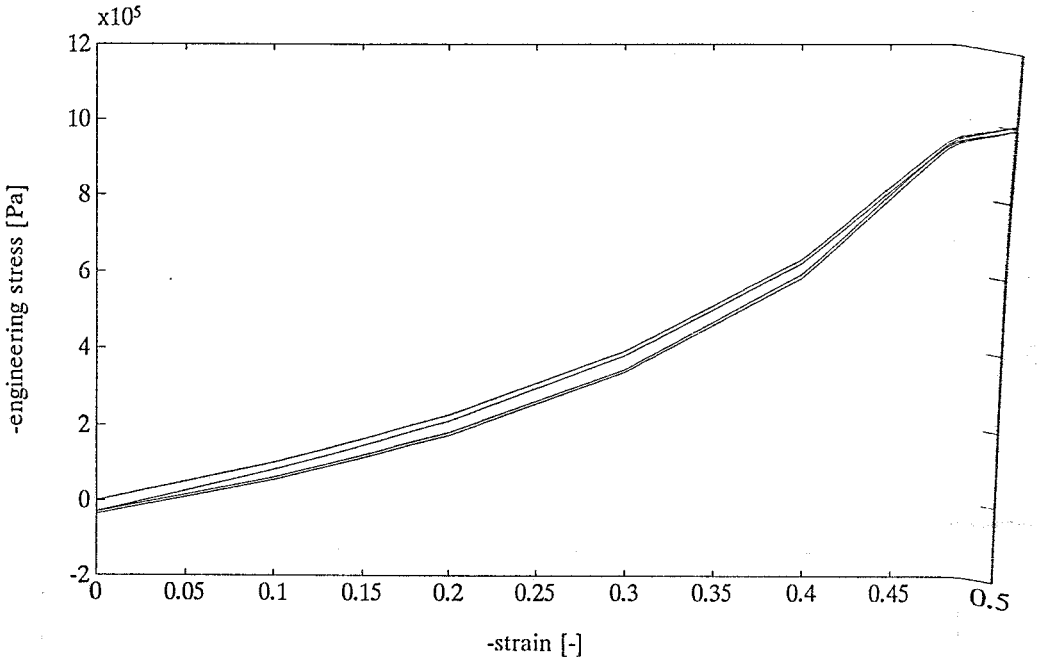

Figure L.2: Hysteresis loop of a butyl rubber cube in uniaxial compression, strain velocity 10 %/min.

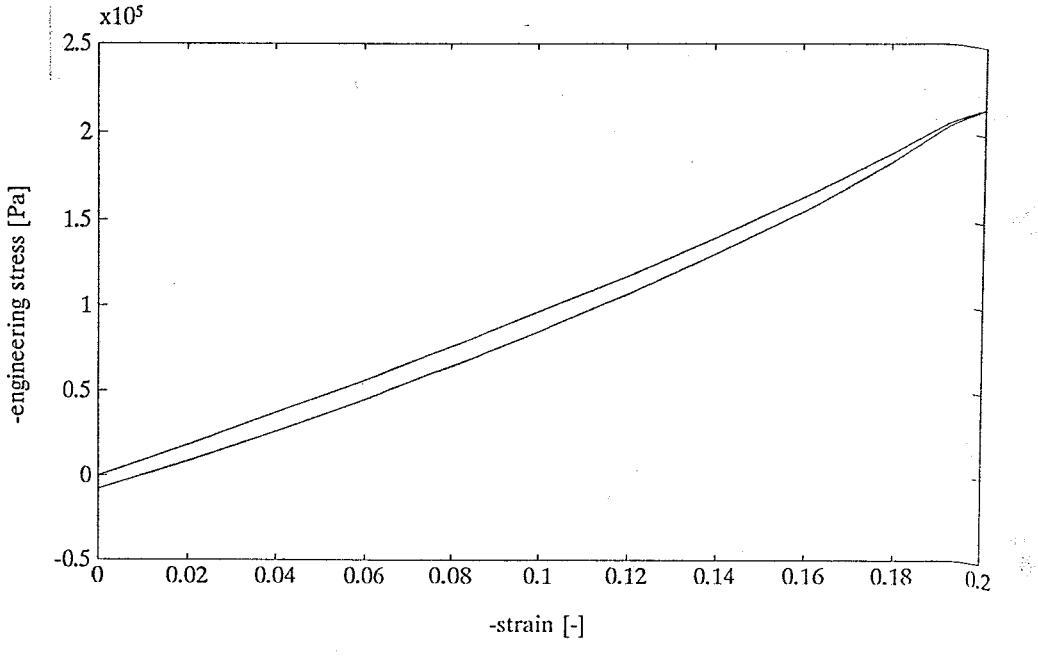

Figure L.3: Hysteresis loop of a butyl rubber pipe in uniaxial compression, strain velocity 10 %/min.

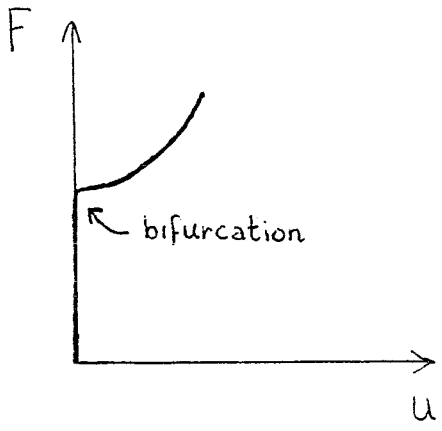

Figure L.4: Force deflection characteristics of a pipe.

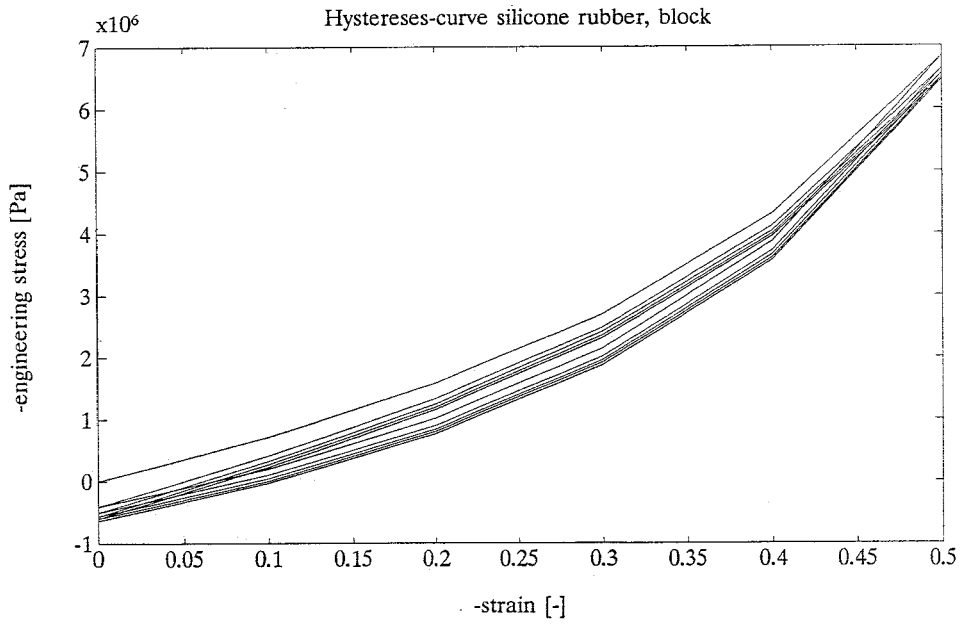

Figure L.5: Hysteresis loop of a silicone rubber cube in uniaxial compression, strain velocity 5000 %/min.

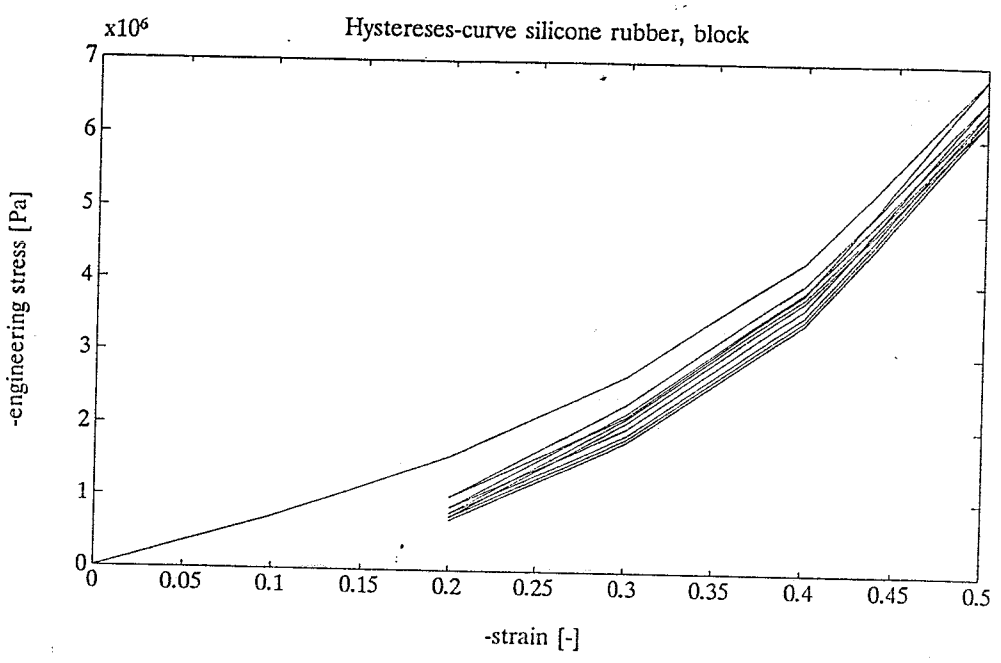

Figure L.6: Hysteresis loop of a silicone rubber cube in uniaxial compression, strain velocity 5000 %/min.

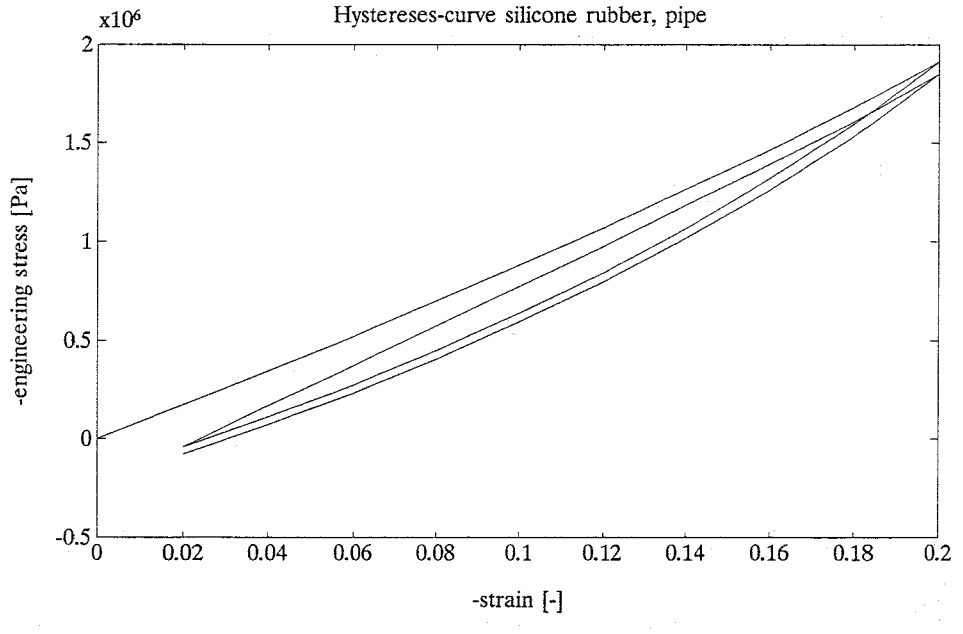

Figure L.7: Hysteresis loop of a silicone rubber pipe in uniaxial compression, strain velocity 5000 %/min.

Appendix M

Derivation of the transfer function for a Maxwell element

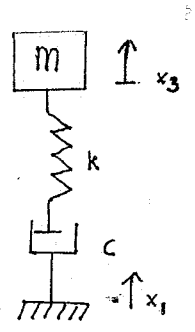

Figure M.1: One Maxwell element.

Figure M.1 represents one Maxwell element. The spring corresponds to a rigidity k and the dashpot to a viscosity c. The assumption is made that the mass is rigid and only displacements in the x-direction are possible. x_1 is the displacement input, x_3 is the displacement output. The transfer function is defined by:

$$T = \frac{\text{output}}{\text{input}} = \frac{x_3}{x_1} \tag{M.1}$$

With the use of a so-called free body diagram the transfer function can be derived. Figure M.2 shows the free body diagram of the Maxwell element. The following set of equations can be derived from this free body diagram.

$$-f_3 = m\,\ddot{x}_3 \tag{M.2}$$

$$f_3 = k\,(x_3 - x_2) \tag{M.3}$$

$$f_2 = f_3 = c(\dot{x}_2 - \dot{x}_1) \tag{M.4}$$

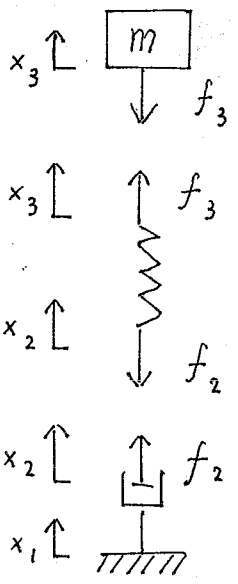

Figure M.2: Free body diagram of the Maxwell element.

From equation M.3 it follows that:

$$x_2 = x_3 - \frac{1}{k} f_3 \tag{M.5}$$

Substitution of equation M.5 in equation M.4 yields:

$$f_3 = c(\dot{x}_3 - \frac{1}{k}\dot{f}_3 - \dot{x}_1) \tag{M.6}$$

The force f_3 can be eliminated by substitution of equation M.2 in the above equation:

$$c\,\dot{x}_1 = \frac{cm}{k} \overset{\cdots}{x}_3 + m\,\ddot{x}_3 + c\,\dot{x}_3 \tag{M.7}$$

Application of Laplace transformation yields:

$$x_1(cs) = x_3(\frac{cm}{k} s^3 + m\,s^2 + c\,s) \tag{M.8}$$

where the Laplace operator s equals $j\,\omega$. The transfer function is then given by:

$$T = \frac{x_3}{x_1} = \frac{c}{\frac{cm}{k}s^2 + ms + c} \tag{M.9}$$

With the use of the program Matlab, Bode-diagrams of the above transfer function can be easily plotted.

The constants k and c occuring in the transfer function of the Maxwell element can be expressed in terms of the experimentally determined relaxation coefficients g_i and relaxation times θ_i.

$$k = 3 \sum_{i=1}^{n} \frac{A}{l_0} g_i \tag{M.10}$$

$$c = \sum_{i=1}^{n} \frac{A}{l_0} g_i \theta_i \tag{M.11}$$

where A represents the sample area and l_0 represents the sample length. Furthermore when shear instead of uniaxial tension is chosen as mode of deformation, the factor 3 should be ommitted from equation M.10.

Appendix N

Bode plots of butyl and silicone rubber

In this appendix the Bode plots as obtained for silicone and butyl rubber are shown. The transmissibility is expressed in decibels. The mass is chosen to equal 80 grams, because this is the weight of the laser module inside an outdoor CD-player. The transfer function of the dampers for the suspension of the laser module inside an outdoor CD-player should have the following characteristics [16]:

- natural frequency $\approx$ 30 Hz.
- peak transmissibility at resonance $\approx$ 5-8 dB.
- Reduction at 100 Hz $\approx$ -20 dB.

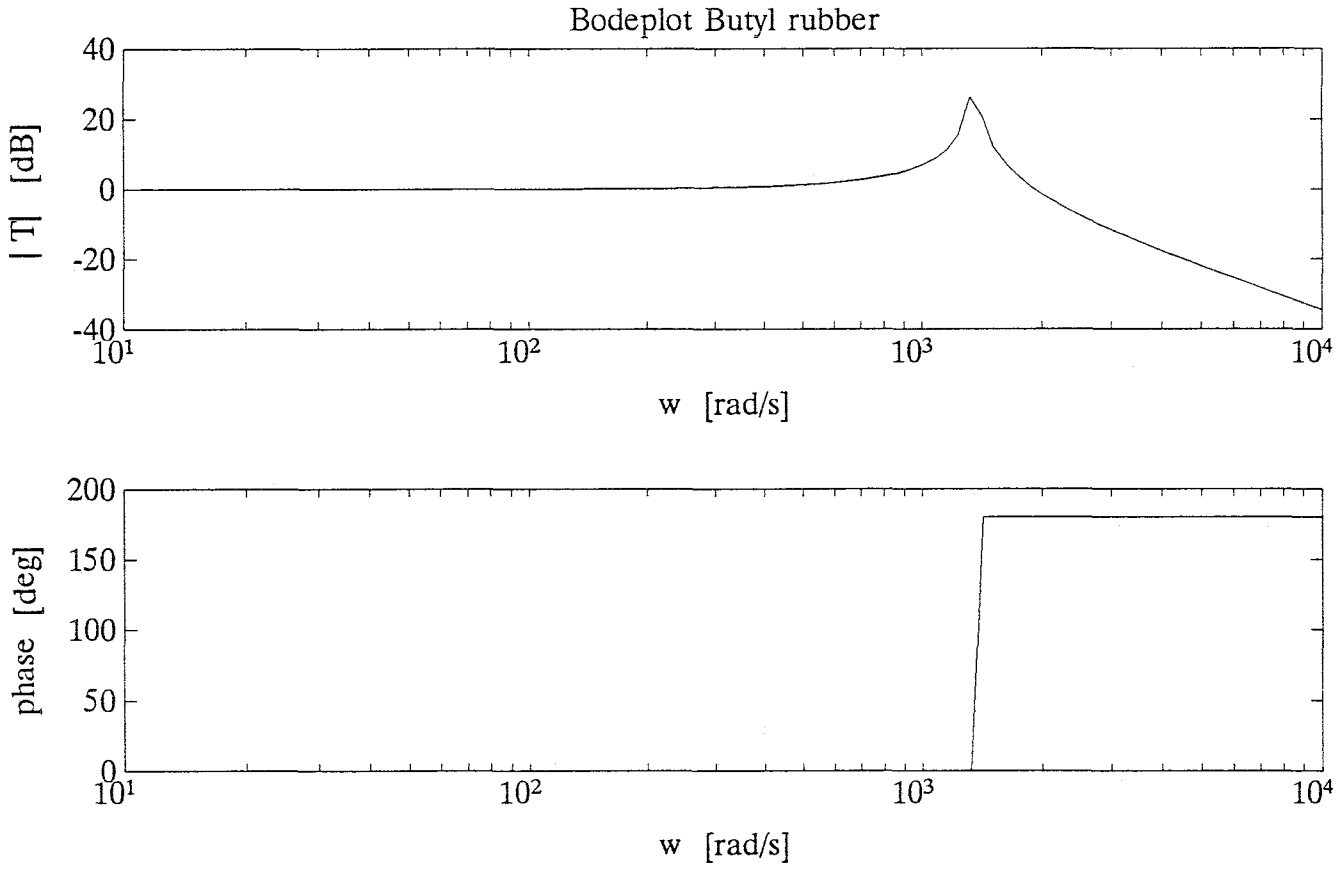

Figure N.1: Bode plot of butyl rubber in uniaxial tension. Sample dimensions: r=4mm, l=16mm

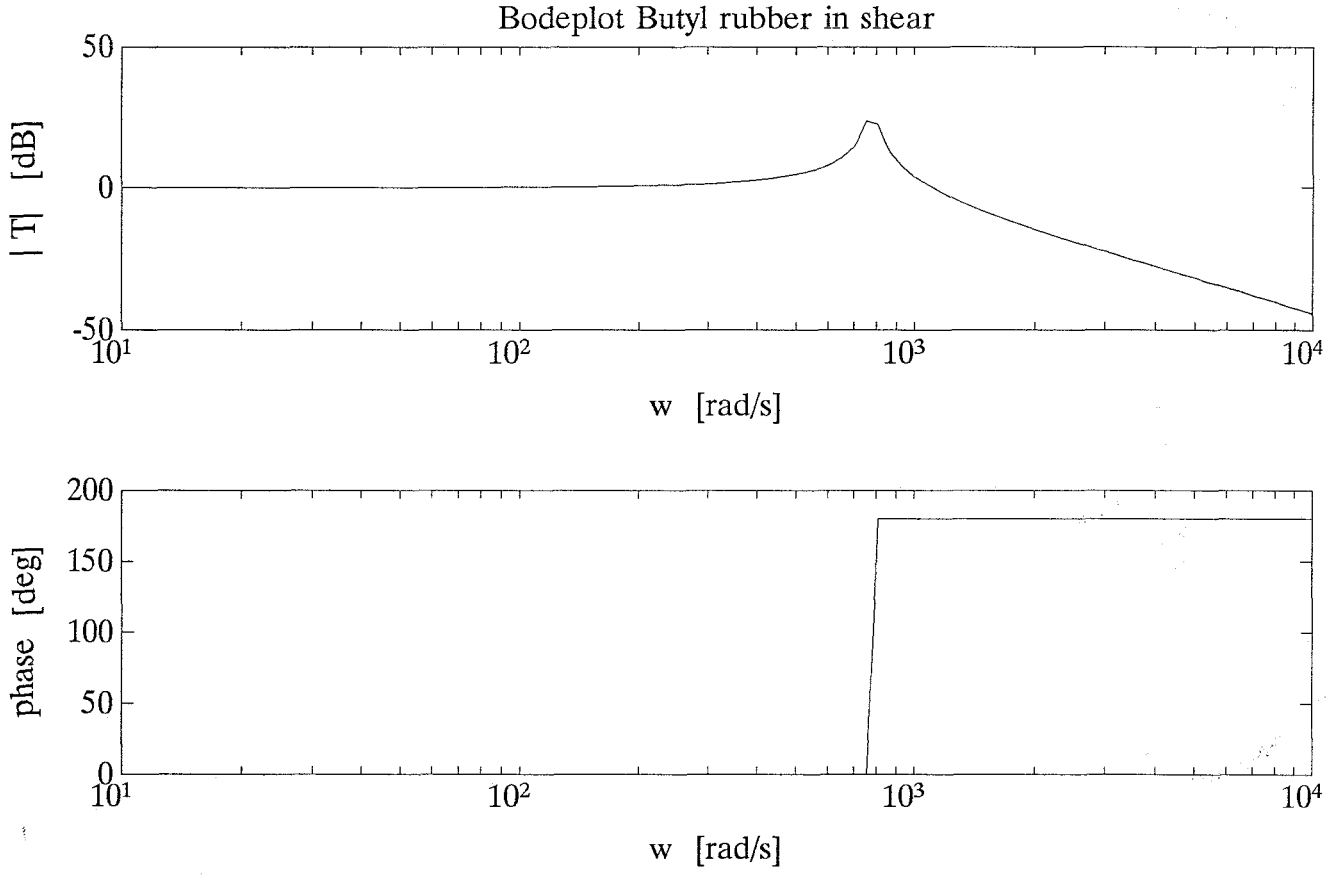

Figure N.2: Bode plot of butyl rubber in shear. Sample dimensions: r=4mm, l=16mm

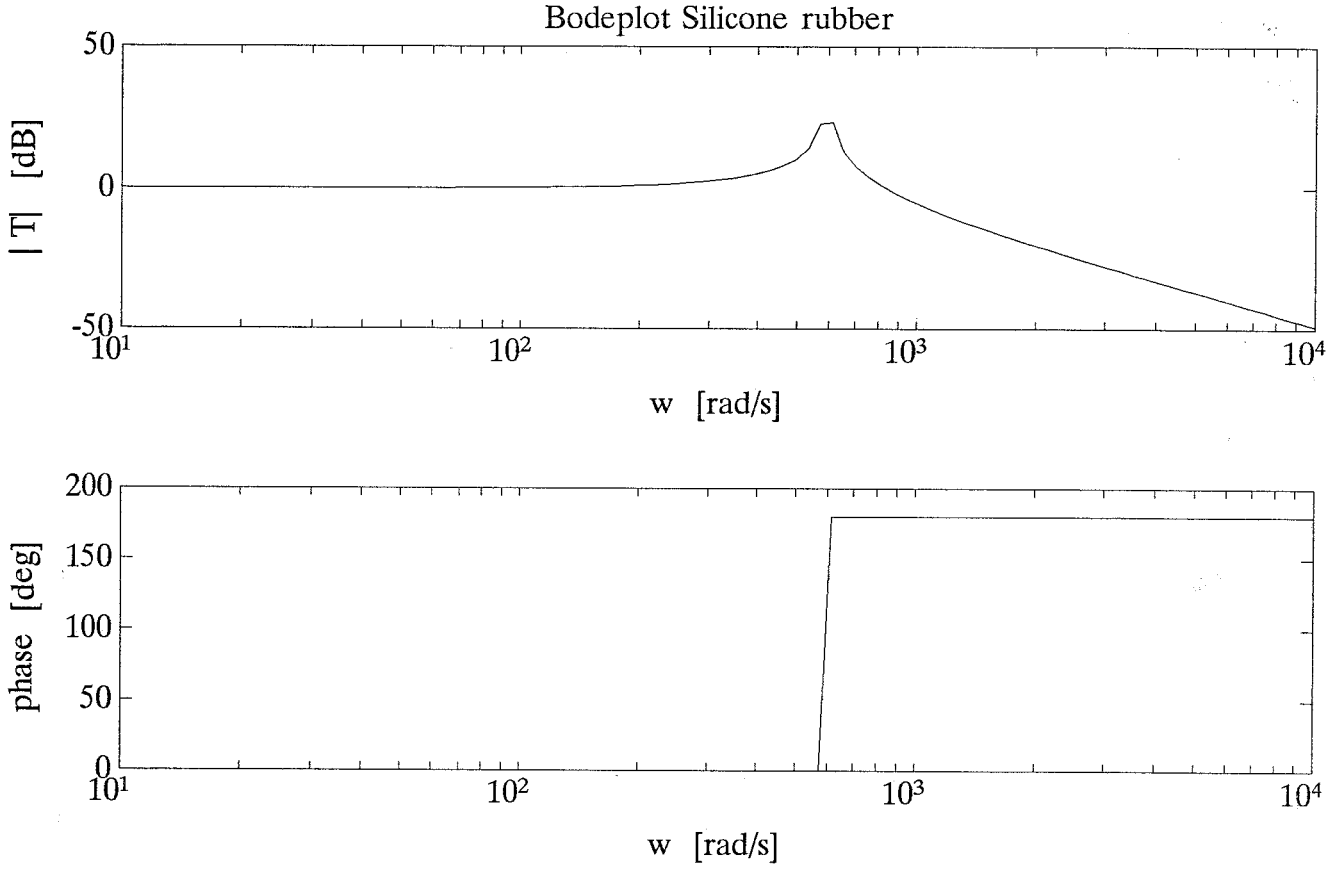

Figure N.3: Bode plot of silicone rubber in uniaxial tension. Sample dimensions: r=4mm, l=16mm

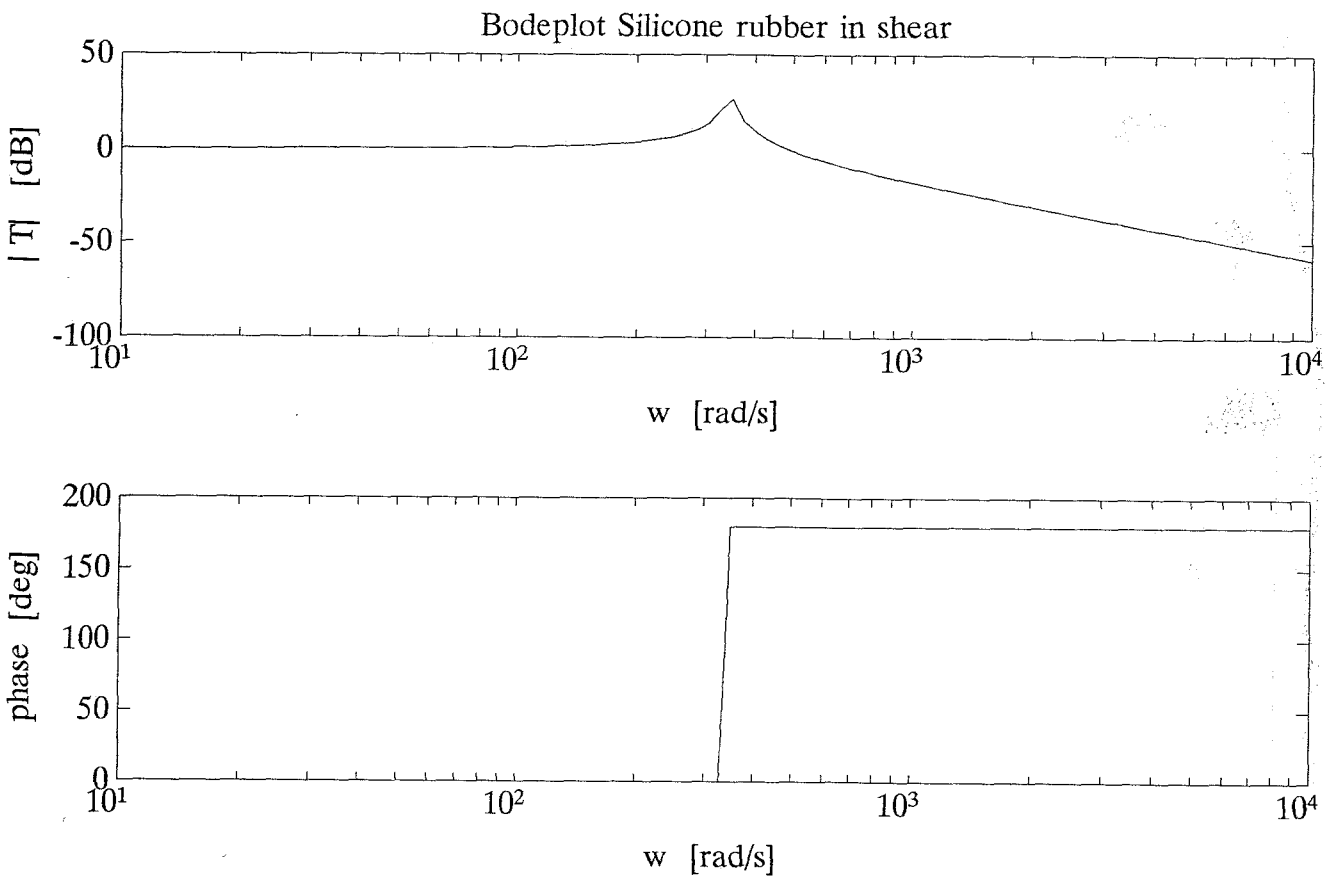

Figure N.4: Bode plot of silicone rubber in shear. Sample dimensions: r=4mm, l=16mm

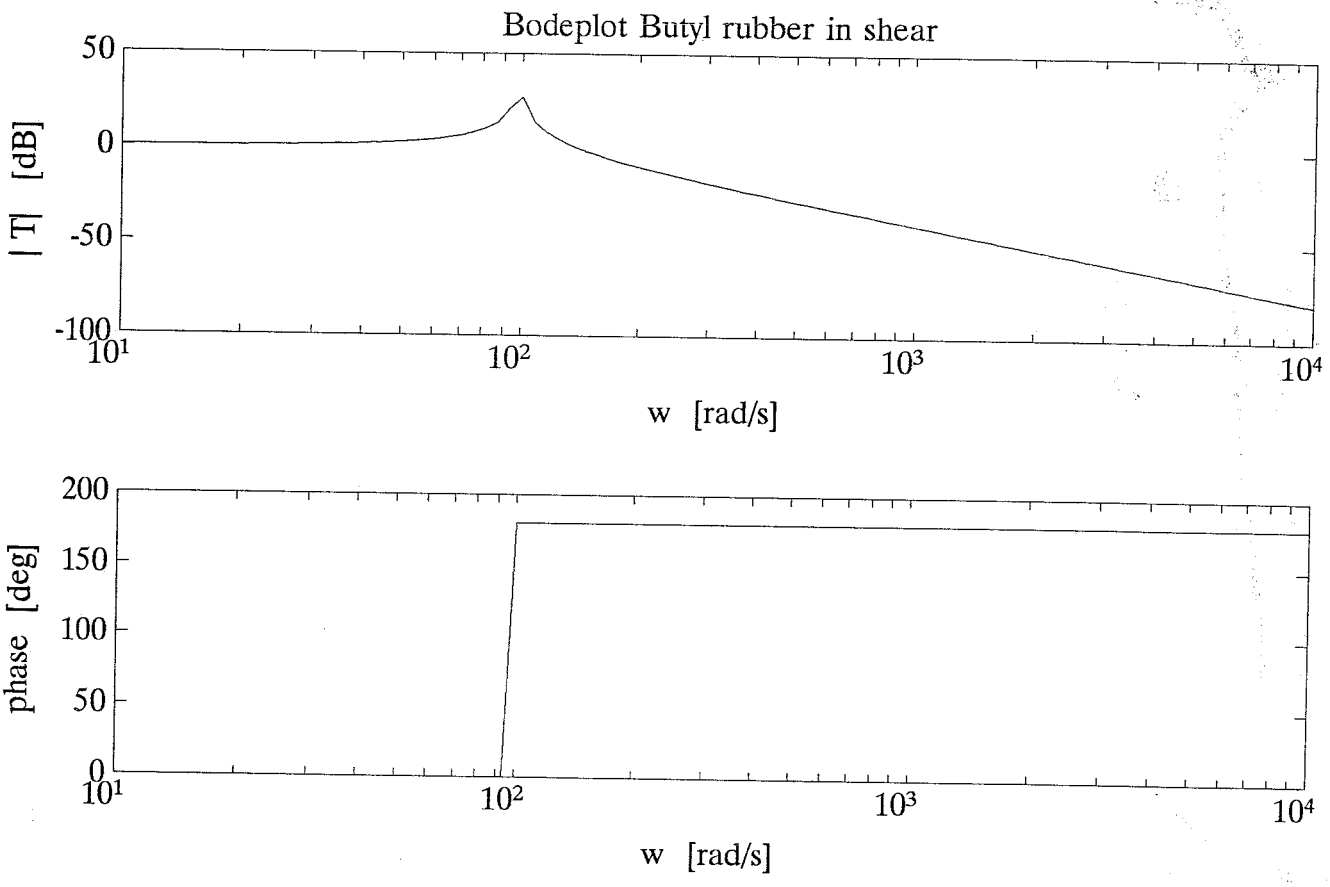

Figure N.5: Bode plot of butyl rubber in shear. Sample dimensions: r=0.5mm, l=16mm

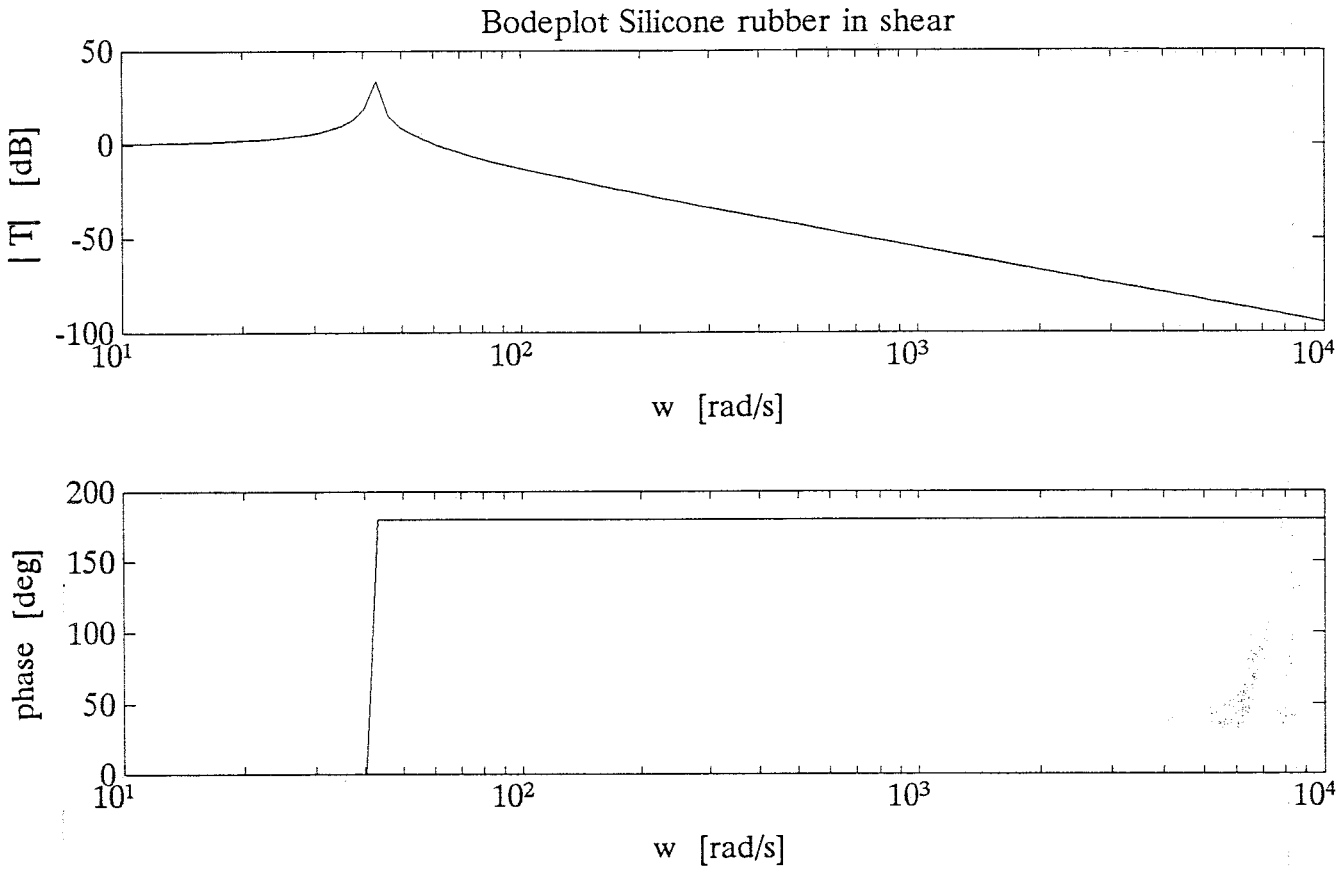

Figure N.6: Bode plot of silicone rubber in shear. Sample dimensions: r=0.5mm, l=16mm